A simple axisymmetric model of magnetosphere-ionosphere coupling currents in Jupiter's polar ionosphere

S. W. H. Cowley, I. Alexeev, E. S. Belenkaya, E. Bunce, C. E. Cottis, Vladimir V. Kalegaev, Jonathan D. Nichols, Renée Prangé, F. J. Wilson

A simple axisymmetric model of magnetosphere-ionosphere coupling currents in Jupiter's polar ionosphere

S. W. H. Cowley,[1] I. I. Alexeev,[2] E. S. Belenkaya,[2] E. J. Bunce,[1] C. E. Cottis,[1] V. V. Kalegaev,[2] J. D. Nichols,[1] R. Prangé,[3] and F. J. Wilson[1]

Received 20 May 2005; revised 1 July 2005; accepted 23 August 2005; published 11 November 2005.

[1] We propose a simple illustrative axisymmetric model of the plasma flow and currents in Jupiter's polar ionosphere which are due both to internal magnetospheric plasma processes and the solar wind interaction. The plasma flow in the model is specified using a combination of observations, previous modeling, and theory, and the ionospheric and field-aligned currents are then calculated. With increasing latitude, the model represents conditions in the inner, middle, and outer magnetosphere on closed field lines and on open field lines mapping to the tail lobes. The model allows us to address three important topics, concerned with the closure of the upward field-aligned currents flowing in the middle magnetosphere region, the energy transfers from planetary rotation to polar upper atmosphere heating and to the magnetosphere, and the relative significance of auroral processes associated with the boundary of open field lines (and hence with the solar wind interaction) and with the middle magnetosphere. It is shown in particular that the energy transfers to the polar upper atmosphere and magnetosphere are of order hundreds of TW each and that discrete auroral precipitation is expected both at the boundary of open field lines and in the middle magnetosphere, though being dominated by the latter. While the initial calculations assume for simplicity a constant ionospheric conductance, we also present a development of the model in which the conductance is self-consistently increased in regions of upward field-aligned current by the precipitation of accelerated electrons. It is shown that this feedback acts to spread the upward current in the region equatorward of the open field line boundary, thus reducing the energy flux and total power of precipitating auroral electrons in this region. At the same time it concentrates the upward current in the equatorward part of the middle magnetosphere, thereby increasing the energy flux and total power of precipitating electrons in this region.

Citation: Cowley, S. W. H., I. I. Alexeev, E. S. Belenkaya, E. J. Bunce, C. E. Cottis, V. V. Kalegaev, J. D. Nichols, R. Prangé, and F. J. Wilson (2005), A simple axisymmetric model of magnetosphere-ionosphere coupling currents in Jupiter's polar ionosphere, *J. Geophys. Res.*, *110*, A11209, doi:10.1029/2005JA011237.

1. Introduction

[2] Momentum and energy are exchanged between the ionospheres and magnetospheres of magnetized planets via the magnetic field that links them, thus setting up large-scale current systems that flow between these regions. For the giant planets Jupiter and Saturn, the current systems associated with two main processes are important. The first is associated with the middle magnetosphere, where planetary angular momentum is transferred to the radially diffusing magnetospheric plasma produced from internal sources such as moon surfaces and atmospheres, to maintain partial corotation of the plasma with the planet [*Hill*, 1979; *Hill et al.*, 1983a; *Vasyliunas*, 1983; *Pontius*, 1997; *Saur et al.*, 2004]. The second is associated with the magnetospheric interaction with the solar wind at the magnetopause boundary [*Hill et al.*, 1983b; *Isbell et al.*, 1984], which is dominant at Earth (see, e.g., the review by *Cowley* [2000], and references therein).

[3] For the Jovian system, which is the topic of the present paper, the main focus of recent research has been on middle magnetosphere currents, following the suggestion by a number of authors that Jupiter's "main oval" auroras are associated with the region of upward directed field-aligned currents in the inner part of the system, carried by downward precipitating magnetospheric electrons [*Bunce and Cowley*, 2001; *Hill*, 2001; *Khurana*, 2001; *Southwood and Kivelson*, 2001]. The main oval at Jupiter is observed to form a bright continuous ring of emission $\sim 1°$ latitude wide at $\sim 15°$ magnetic colatitude, which is relatively steady in time [*Satoh et al.*, 1996; *Clarke et al.*, 1998, 2004; *Prangé et al.*, 1998; *Vasavada et al.*, 1999;

[1]Department of Physics and Astronomy, University of Leicester, Leicester, UK.
[2]Institute of Nuclear Physics, Moscow State University, Moscow, Russia.
[3]Observatoire de Paris, Meudon, France.

0148-0227/05/2005JA011237

Pallier and Prangé, 2001; *Grodent et al.*, 2003a]. According to magnetic models, this ring maps in the equatorial plane to the inner part of the middle magnetosphere, at radial distances of $\sim$20–30 R_J. (R_J is Jupiter's equatorial radius of $\sim$71,400 km.) Spectral analysis of the emission at ultraviolet (UV) wavelengths shows that the emission is due to precipitation of electrons with energies $\sim$50–150 keV, whose number flux at the ionosphere is equivalent to field-aligned current densities of $\sim$0.1–0.4 μA m^{-2} [*Gustin et al.*, 2004].

[4] With regard to theoretical modeling, although the current system is implicit in the earlier calculations of *Hill* [1979] and *Pontius* [1997], the form of the middle magnetosphere currents associated with radial outward transport from the Io plasma torus at Jupiter was first calculated explicitly by *Hill* [2001] and *Cowley and Bunce* [2001]. *Hill* [2001] determined the currents in an idealized model in which a steady plasma outflow from the torus takes place in a dipole planetary magnetic field, this representing the original model of *Hill* [1979]. For typical plasma parameters it was found that a ring of upward field-aligned current is centered at $\sim$10° magnetic colatitude in the ionosphere, the current then reversing to downward in a region surrounding the magnetic pole if the model is taken to extend to infinity in the equatorial plane. The upward and downward currents then close via radially outward current flow across the field lines in the equatorial plasma, and equatorward directed Pedersen currents in the ionosphere. The torques associated with the cross-field currents self-consistently transfer planetary angular momentum from the atmosphere and coupled ionosphere, to the outwardly diffusing equatorial plasma. *Cowley and Bunce* [2001], on the other hand, employed a realistic current sheet model of the middle magnetosphere field, together with an empirical model of the plasma angular velocity based on experimental data and the results of *Pontius* [1997]. They found that use of a more realistic poloidal field results in upward field-aligned current densities at the ionosphere that are an order of magnitude larger than for a dipole field, comparable to the observed values quoted above, which map to a narrow latitudinal band around $\sim$15° colatitude where the main oval auroras are found. Using the kinetic theory of *Knight* [1973], they also showed that the currents require the field-aligned acceleration of magnetospheric electrons to energies of $\sim$100 keV, thereby producing precipitating electron energy fluxes of appropriate magnitude to explain the main oval UV emissions. *Cowley et al.* [2002, 2003a] subsequently showed that similar results are obtained if self-consistently computed plasma angular velocity profiles are employed rather than empirical models, while *Nichols and Cowley* [2003] confirmed the general validity of the conclusions over wide but realistic ranges of the system parameters. Recent developments have included the effect of feedback of the electron precipitation on ionospheric conductance [*Nichols and Cowley*, 2004], and the self-consistent inclusion of the accelerating field-aligned voltages in the dynamical problem where it is shown that these produce only small effects in the Jovian context [*Nichols and Cowley*, 2005]. A ubiquitous feature of these realistic middle magnetosphere models, however, is that the field-aligned current is found to be directed upward from the ionosphere to the magnetosphere throughout the region, being concentrated into the inner part, mapping to $\sim$20–40 R_J in the equatorial plane, when conductance feedback effects are included. The question of current closure in the poleward region, mapping to the outer magnetosphere and tail, is not described in these models and is thus left as an open issue.

[5] Flows and currents in the higher-latitude regions of Jupiter's ionosphere, poleward of the main oval, have by comparison been relatively little studied, though observations show that intermittent UV emissions do occur in this region [e.g., *Prangé et al.*, 1998; *Grodent et al.*, 2003b]. Indeed, *Pallier and Prangé* [2001] have discussed the presence of faint and partial "inner ovals" or "arcs," the most poleward of which border an aurorally dark region suggested to be the polar cap region of open field lines. A bright auroral "spot" is also often observed near the equatorward edge of this most poleward emission region near magnetic noon, which has been suggested to be associated with the dayside cusp [*Pallier and Prangé*, 2001, 2004]. On occasion the emission from this region has been observed to "flare" to great intensity in the UV [*Waite et al.*, 2001], and X rays can also be emitted from an adjacent region [*Elsner et al.*, 2005]. *Bunce et al.* [2004] have suggested that the "cusp spot" effects are produced by the localized field-aligned current system associated with pulsed magnetopause reconnection, in which electrons and ions are accelerated along the field lines in adjacent regions of upward and downward directed field-aligned current.

[6] A qualitative overall picture of the plasma flow and currents in the Jovian polar ionosphere incorporating these features has recently been presented by *Cowley et al.* [2003b]. In this picture the plasma rigidly corotates with the planet at lower latitudes mapping to the inner magnetosphere, the plasma angular velocity then falling with increasing latitude across the region mapping to the middle magnetosphere to some fraction of rigid corotation in the outer magnetosphere, as indicated by magnetospheric plasma observations, and then to almost stagnant conditions (in the inertial frame) on open field lines mapping to the tail lobes, in conformity with the infrared (IR) Doppler observations of *Stallard et al.* [2003]. In this paper we present a quantitative development of this picture, simplified to conditions of axisymmetry for ease of theoretical development. Although simplistic, this model should nevertheless represent the zeroth-order variations of the flow and current with latitude, thus allowing us for the first time to address the issue of overall current closure (other than in the idealized dipole field model of *Hill* [2001]). It also allows us to make estimates of the planetary rotational energy transferred via these current systems to the magnetosphere and to atmospheric heating, the latter potentially contributing to an understanding of the outstanding issue of the elevated temperatures observed in the Jovian thermosphere [*Miller et al.*, 2000; *Yelle and Miller*, 2004]. Furthermore, the model also allows an assessment of the relative significance of the currents and discrete auroral precipitation associated with middle magnetosphere processes and the solar wind interaction, though in the axisymmetric approximation the local time-dependent features associated with the cusp or "substorm" currents (associated with time-dependent reconnection at the dayside magnetopause and in the tail, respectively) cannot be represented. A model of this nature was recently pre-

sented by *Cowley et al.* [2004b] for Saturn's magnetosphere-ionosphere coupling currents, based on an initial qualitative discussion by *Cowley et al.* [2004a]. In this case the results indicate that auroral processes at Saturn are dominated by the solar wind interaction rather than by middle magnetosphere effects, thus confirming the earlier results of *Cowley and Bunce* [2003b]. Here we will present a related model for Jupiter, where the opposite appears to be the case.

2. Theoretical Background

2.1. Basic Assumptions

[7] The object of the work presented here is to develop the simplest overall model that represents the zeroth-order flows and currents in Jupiter's polar ionosphere. The principal simplification made is that the system is axisymmetric about the magnetic axis as indicated above, such that the flows considered are wholly azimuthal, and can thus be discussed in terms of the degree of departure from rigid corotation with the planet. While axisymmetry seems appropriate to a description of the largely rotational flows in the middle magnetosphere, as assumed in all the theoretical studies cited above, it is perhaps less obviously appropriate in the region of open field lines where only strongly subcorotational flow is included in the description, and no representation is made of the local time-dependent flows associated with the Dungey cycle. However, while description of some significant phenomena is thereby excluded, such as the effect of localized cusp and substorm currents as mentioned above, the axisymmetric approximation still represents a useful lowest-order description in this region, as will be discussed further below.

[8] Four theoretical ingredients are required to develop the model. The first is a model of the plasma angular velocity ω, defined in the ionosphere as a function of colatitude θ_i. The functional form of $\omega(\theta_i)$ is specified at the outset, based on observations, previous modeling, and theory, and is used to calculated the ionospheric electric field and currents. Details will be given in the following section. The second is a model of Jupiter's magnetic field in the current-carrying layer of the ionosphere. This layer is taken to lie $\sim$500 km above the 1 bar pressure level according to the results of *Millward et al.* [2002], which itself lies at a polar radius of 66,854 km. We thus take a fixed polar ionospheric radius R_i equal to 67,350 km. In principle the polar-flattened spheroidal figure of the planet could be included in the calculation, as was incorporated in the Saturn model by *Cowley and Bunce* [2003b] and *Cowley et al.* [2004b]. Here, however, we focus solely on the region poleward of $\sim$20° colatitude where corotation breaks down, such that this is a minor effect. According to the VIP4 magnetic model of *Connerney et al.* [1998], based on spacecraft and auroral data, the polar ionospheric magnetic field varies significantly with latitude, longitude, and between hemispheres. Since longitude effects clearly cannot be incorporated into an axisymmetric model, and since these are comparable in magnitude to the latitude and hemispheric variations, we have chosen instead to take the simplest possible model, that is, a radial field of fixed representative magnitude B_i. On the basis of the VIP4 model, we have chosen B_i to be 1.1×10^{-3} T. The third ingredient is a model for the ionospheric Pedersen conductance, from which the Pedersen currents can be calculated for a given plasma flow model. Account also has to be taken of the effect of thermospheric winds excited by ion-neutral collisions in the Pedersen layer, as will be discussed further below. In the next section we present results for a fixed representative value of the Pedersen conductance, while in section 4 we consider the effect of precipitation-induced enhancements in the conductance in regions of upward field-aligned current, based on the modeling results of *Millward et al.* [2002]. Hall currents are also driven eastward for subcorotational plasma flow, but in an axisymmetric model these close wholly in the ionosphere and do not contribute to the magnetosphere-ionosphere coupling considered here. The fourth and final ingredient is a model which relates field-aligned currents to auroral electron precipitation, allowing field-aligned acceleration voltages and precipitating electron energy fluxes to be estimated. Here, in common with previous analyses, we employ the kinetic theory of *Knight* [1973], combined with observed typical properties of the "source" electrons in the magnetosphere.

[9] With this introduction, we now present the basic theory governing the model, specifically concerning the relation of the flow and current systems, energy transfer, and auroral acceleration. Other items will be dealt with in subsequent sections, as indicated above. Since the basic theory has been discussed in several recent related papers [e.g., *Cowley et al.*, 2004b], only a brief development is provided here, sufficient to serve the needs of self-containment.

2.2. Ionospheric and Field-Aligned Current Systems

[10] Three angular velocities are introduced in the calculation of the ionospheric currents. These are the angular velocity of the planet Ω_J (equal to 1.76×10^{-4} rad s^{-1}), the angular velocity of the subcorotating plasma ω, and the angular velocity of the neutral atmosphere in the Pedersen layer, Ω_J^*, which we expect to lie intermediate between ω and Ω_J due to the frictional drag of ion-neutral collisions [*Huang and Hill*, 1989]. In this case we can write for some $0 < k < 1$

$$(\Omega_J - \Omega_J^*) = k(\Omega_J - \omega), \tag{1}$$

where modeling studies presented by *Millward et al.* [2005] indicate values $k \approx 0.5$ under Jovian auroral conditions. For subcorotating plasma the height-integrated Pedersen current intensity i_P is then directed equatorward in both hemispheres, given by

$$i_P(\theta_i) = \Sigma_P E_i(\theta_i) = \Sigma_P \rho_i(\Omega_J^* - \omega)B_i, \tag{2}$$

where Σ_P is the ionospheric Pedersen conductance (the Pedersen conductivity integrated in height through the ionosphere), E_i is the electric field in the neutral atmosphere rest frame, and $\rho_i = R_i \sin\theta_i$ is the perpendicular distance to the axis of symmetry. Substitution of Ω_J^* from equation (1) into equation (2) then yields

$$i_P(\theta_i) = \Sigma_P^* \rho_i(\Omega_J - \omega)B_i, \tag{3}$$

where Σ_P^* is the "effective" value of the ionospheric Pedersen conductance

$$\Sigma_P^* = (1-k)\Sigma_P, \tag{4}$$

reduced from the true value by the "slippage" of the neutral atmosphere from rigid corotation. Integrating in azimuth yields the "total" ionospheric Pedersen current flowing at colatitude θ_i

$$I_P(\theta_i) = 2\pi\rho_i i_P(\theta_i) = 2\pi\Sigma_P^*\rho_i^2(\Omega_J - \omega)B_i. \tag{5}$$

Current continuity then requires that latitudinal variations in $I_P(\theta_i)$ be accompanied by field-aligned currents flowing between the ionosphere and magnetosphere. The field-aligned current density flowing just above the ionosphere is given by

$$j_{\|i} = -\frac{1}{2\pi R_i^2 \sin\theta_i}\frac{dI_P}{d\theta_i}, \tag{6}$$

where the sign is applicable to the northern hemisphere where the ionospheric field points outward from the planet.

2.3. Energy Transfer

[11] As indicated above, one of the concerns of this study is to obtain overall estimates of the energy extracted from planetary rotation and either transferred to the magnetosphere or dissipated as heat in the upper atmosphere. The total power per unit area of ionosphere extracted from planetary rotation by the above current system [e.g., *Hill et al.*, 1983b; *Isbell et al.*, 1984; *Hill*, 2001] is given by

$$p = \Omega_J\tau = \Omega_J\rho_i i_P B_i, \tag{7}$$

where τ is the torque per unit area of ionosphere about the axis of symmetry. The torque is associated with the height-integrated $\boldsymbol{j} \times \boldsymbol{B}$ force, which in the ionosphere is directed (for subcorotation) opposite to planetary rotation. Of this total, the amount transferred to the magnetosphere via the magnetic field is

$$p_M = \omega\tau = \omega\rho_i i_P B_i, \tag{8}$$

which maintains partial corotation of radially diffusing plasma of internal origin on closed field lines and twists the tail field on open field lines. The remainder

$$p_A = (\Omega_J - \omega)\tau = (\Omega_J - \omega)\rho_i i_P B_i, \tag{9}$$

is dissipated as heat in the upper atmosphere. As pointed out by *Smith et al.* [2005], the latter power consists of two components. The first is the direct "Joule heating" in the Pedersen layer at the rate

$$p_J = \boldsymbol{i}_P \cdot \boldsymbol{E}_i = (\Omega_J^* - \omega)\rho_i i_P B_i, \tag{10}$$

while the second is the "ion drag" power associated with subcorotation of the neutral atmosphere due to the torque

$$p_D = (\Omega_J - \Omega_J^*)\tau = (\Omega_J - \Omega_J^*)\rho_i i_P B_i, \tag{11}$$

which is viscously dissipated to heat at some level in the atmosphere. Adding equations (10) and (11) then yields the total power per unit area dissipated to heat in the atmosphere given by equation (9). We note that this total power, which can also be expressed as

$$p_A = \frac{i_P^2}{\Sigma_P^*} \tag{12}$$

through equation (3), is the quantity written as p_J^* by *Cowley et al.* [2004b] and discussed as an upper limit to the atmospheric Joule heating rate (at Saturn) in the limit of a rigidly corotating neutral atmosphere. When the "ion drag" power is added, however, this quantity also becomes the true total power per unit area dissipated to heat in the upper atmosphere, as noted by *Smith et al.* [2005]. Total powers are then obtained by integration of the above quantities over appropriate areas of the ionosphere.

2.4. Auroral Acceleration and Energy Flux

[12] Another concern of the study is to examine the model regions of upward field-aligned current with regard to acceleration of downward precipitating electrons and the formation of discrete auroras. The maximum current density that can be carried by downward precipitating electrons without field-aligned acceleration is

$$j_{\|i0} = eN\left(\frac{W_{th}}{2\pi m_e}\right)^{1/2}, \tag{13}$$

with a corresponding precipitating energy flux (energy per unit area per unit time) of

$$E_{f0} = 2NW_{th}\left(\frac{W_{th}}{2\pi m_e}\right)^{1/2}. \tag{14}$$

In these expressions the magnetospheric source electron population (charge e and mass m_e) has been assumed to be an isotropic Maxwellian of density N and thermal energy W_{th} (equal to k_BT where T is the temperature and k_B is Boltzmann's constant) and that the precipitating population has a full downward going loss cone and an empty upward going loss cone. If the upward current required by equation (6) is larger than $j_{\|i0}$ given by equation (13), then a field-aligned voltage must be present which accelerates the electrons into the ionosphere. According to *Knight*'s [1973] kinetic theory, the minimum field-aligned voltage required is

$$\Phi_{\|\min} = \frac{W_{th}}{e}\left(\left(\frac{j_{\|i}}{j_{\|i0}}\right) - 1\right), \tag{15}$$

this value being appropriate if the "top" of the voltage drop is located well above the minimum radial distance given by

$$\left(\frac{r_{\min}}{R_i}\right) \approx \left(\frac{j_{\|i}}{j_{\|i0}}\right)^{1/3}, \tag{16}$$

where we have assumed as a sufficient approximation that the field strength drops as the inverse cube of the distance along

the polar field lines. Equation (15) also assumes that the voltage drop is sufficiently compact along the field lines that electrons do not mirror before experiencing the full voltage. The enhanced precipitating electron energy flux corresponding to equation (15) is then

$$E_f = \frac{E_{f0}}{2}\left(\left(\frac{j_{\|i}}{j_{\|i0}}\right)^2 + 1\right), \tag{17}$$

following *Lundin and Sandahl* [1978]. Here we will thus employ equations (15)–(17) to estimate the electron acceleration conditions and precipitating energy fluxes in regions of upward field-aligned current, using typical observed values of the magnetospheric electron source parameters.

[13] We also wish to estimate the UV auroral output from the precipitating electron input, both with regard to auroral brightness (photon flux) and total energy. The auroras are excited by primary and secondary electron impact on atmospheric atomic and molecular hydrogen, which produces ~10 eV UV photons, corresponding to the atomic hydrogen Lyman alpha line and the molecular hydrogen Lyman and Werner bands. The overall energy efficiency of these processes is ~15% [*Waite et al.*, 1983; *Rego et al.*, 1994], such that 1 mW m^{-2} of precipitating electron input yields ~10 kR of UV photon production in the auroral atmosphere. However, part of this photon flux is absorbed by hydrocarbons overlying the auroral source, such that the emergent UV flux will generally be less than this, depending on the altitude of production and hence on the energy of the primary auroral electrons. For 1 mW m^{-2} of input power, such absorption reduces the UV output to ~8 kR in the case of 10 keV electron primaries and to ~3 kR for 100 keV primaries.

3. Jupiter Model With Constant Ionospheric Conductance

3.1. Plasma Angular Velocity Model

[14] The most significant input to our calculation is the choice of plasma angular velocity model, which is specified at the outset on the basis of observations, previous modeling, and theory. In keeping with the overall objectives outlined in section 2.1 above, our aim has been to develop the simplest model that reasonably describes the large-scale plasma flow. As in the corresponding Saturn model [*Cowley et al.*, 2004b], we consider the flow in four regions. With increasing latitude in the ionosphere, these correspond to the inner, middle, and outer magnetosphere on closed field lines, and the open field region mapping to the tail. In this context, the "inner" magnetosphere is taken to be the region where the plasma near-rigidly corotates with the planet, extending in the equatorial plane to radial distances of ~20 R_J [*Belcher*, 1983; *Sands and McNutt*, 1988; *Nichols and Cowley*, 2004]. According to empirical magnetic models, this equatorial distance maps in the ionosphere to a colatitude of ~16° [e.g., *Connerney et al.*, 1981; *Nichols and Cowley*, 2004]. We thereby do not include in the model the minor departures from rigid corotation in the Io plasma torus itself at larger colatitudes (~23°), which are due to local plasma production and pickup [e.g., *Pontius and Hill*, 1982; *Brown*, 1994]. Nor do we include the larger but more localized effects associated with the direct moon-plasma interactions [e.g., *Hill and Vasyliunas*, 2002]. Beyond ~20 R_J in the equatorial plane the plasma angular velocity then falls continuously with increasing radial distance across the middle magnetosphere (the region containing the azimuthal equatorial current sheet), reaching some fraction of rigid corotation at its outer edge at radial distances of several tens of R_J, depending on solar wind conditions and the state of extension of the magnetosphere. For the relatively compressed magnetosphere observed by Voyager 2, *Kane et al.* [1995] found plasma angular velocities of around half of rigid corotation at the outer edge of the middle magnetosphere on the dayside inbound pass (at ~45 R_J), while at a similar local time *Laxton et al.* [1997] found lower angular velocities of around a quarter of rigid corotation for the more extended magnetosphere observed by Ulysses (at ~70 R_J). Realistic middle magnetosphere models typically provide values within the same range at these distances [e.g., *Nichols and Cowley*, 2004], as do more recent experimental estimates based on Galileo data [*Krupp et al.*, 2001]. The latter data also suggest a dawn-dusk local time asymmetry with higher flow speeds at dawn compared with dusk, though this cannot be represented within the axisymmetric framework adopted here. We will, however, consider two representative models in which the flow falls either to a half or to a quarter of rigid corotation at the outer edge of the middle magnetosphere. We may then consider these models to represent either a compressed or an expanded system, respectively, since generally we would expect higher angular velocities to prevail in a more compressed system [*Southwood and Kivelson*, 2001; *Cowley and Bunce*, 2003a]. Empirical magnetic models then indicate that the outer edge of the middle magnetosphere maps in the ionosphere to a colatitude of ~15°, that is, the fall in angular velocity across the middle magnetosphere takes place over ~1° of colatitude in the ionosphere between ~15° and ~16°, in conformity with previous studies [*Cowley et al.*, 2002; *Nichols and Cowley*, 2003, 2004]. The amount of magnetic flux threading the current sheet between ~20 R_J and its outer edge at several tens of R_J is thus ~150 GWb.

[15] The outer magnetosphere in this model then corresponds to the layer of magnetic flux adjacent to the magnetopause where no azimuthal current sheet is evident, which *Cowley et al.* [2003b] have proposed is formed by the return flow of closed flux tubes from the tail to the dayside magnetopause, principally via dawn, in the Dungey cycle. The nature of this layer will thus depend on local time, though this also cannot be represented directly. Instead we represent the outer magnetosphere as a layer of approximately uniform angular velocity located poleward of the main oval. In the corresponding Saturn model [*Cowley et al.*, 2004b], evidence from Voyager data suggested that the angular velocities in this layer somewhat exceeded that of the outer middle magnetosphere. However, available evidence at Jupiter suggests instead that angular velocities in the two regions are comparable with each other [e.g., *Kane et al.*, 1995]. For simplicity therefore we take the flow in the outer magnetosphere to plateau at the value in the outer middle magnetosphere, at a half and a quarter of rigid corotation in our two models, respectively, and to extend

at these values to the open-closed field line boundary (i.e., the magnetopause). The colatitude of the latter boundary relates to the amount of open flux in the tail, which is probably a somewhat variable quantity depending on interplanetary conditions and the solar wind interaction. Here we take the open flux in the system to be 500 GWb, comparable with but somewhat larger than the ~320 GWb employed in the magnetic models presented by *Alexeev and Belenkaya* [2005] and *Belenkaya et al.* [2005]. With the value of 500 GWb, the (axisymmetric) open-closed field line boundary then lies at a colatitude of ~10.25° in the ionosphere. The flux in the outer magnetosphere, between the open-closed boundary and the outer limit of the middle magnetosphere at ~15°, is then a further ~500 GWb. The open flux corresponds, for example, to a tail field of ~1.5 nT in a lobe of radius ~200 R_J, while the outer magnetosphere flux corresponds to a field of ~10 nT in a layer which is ~15 R_J wide adjacent to the magnetopause. Such values do not seem unreasonable in terms of observations [e.g., *Acuña et al.*, 1983].

[16] Within the region of open field lines the flow has two components, rotation driven by ion-neutral collisions in the ionosphere which twists the open tail field lines, and the flow associated with the Dungey cycle. The degree to which the open field lines rotate within the tail is a matter of some uncertainty at present and has been discussed, for example, by *Belenkaya* [2004]. Here, however, we follow the description of *Isbell et al.* [1984], whose analysis using a simplified geometry suggests that the rotation takes place at a uniform angular velocity in the inertial frame given by

$$\left(\frac{\omega}{\Omega_J}\right) = \frac{\mu_0 \Sigma_P^* V_{SW}}{1 + \mu_0 \Sigma_P^* V_{SW}}, \tag{18}$$

where μ_0 is the permeability of free space and V_{SW} is the velocity of the solar wind. The fixed value of Σ_P^* that will be employed in this section is 0.2 mho, as will be discussed further below. With this value we have $\mu_0 \Sigma_P^* V_{SW} \approx 0.1$ for a solar wind speed of 400 km s^{-1} so that $(\omega/\Omega_J) \approx 0.09$ in the open field region. That is, the flow within this region is strongly subcorotational, in conformity with the almost "stagnant" plasma conditions observed in IR Doppler data in the high-latitude "dark polar region" [*Stallard et al.*, 2003]. With this value for the angular velocity, the plasma flow at the outer boundary of the open field region, for example, is ~200 m s^{-1}, compared with ~2 km s^{-1} for rigid corotation. We cannot include the local time-dependent Dungey cycle flow within our axisymmetric model but note that *Cowley et al.* [2003b] have estimated the antisunward flow to be only ~50–100 m s^{-1} on open field lines under typical conditions. These flows are therefore at most comparable with the subcorotational flow in the inertial frame and do not affect the conclusion of near-stagnant plasma conditions in this region. The ionospheric current, however, is determined by the plasma flow in the neutral atmosphere rest frame, such that the most significant effect is the strongly subcorotational nature of the flow as described by the model. The Dungey cycle flow, which is not included, then represents only a small correction.

[17] With increasing colatitude from the pole therefore the angular velocity in our model increases monotonically from ~10% of rigid corotation on open field lines to full rigid corotation equatorward of ~16°, in two steps. The first increase corresponds to the open-closed field line boundary and the second to the middle magnetosphere (outside ~20 R_J). The convenient functional form chosen to represent this behavior is

$$\begin{aligned}\left(\frac{\omega(\theta_i)}{\Omega_J}\right) = {} & \left(\frac{\omega}{\Omega_J}\right)_{Open} \\ & + \frac{1}{2}\left[\left(\frac{\omega}{\Omega_J}\right)_{OM} - \left(\frac{\omega}{\Omega_J}\right)_{Open}\right]\left[1 + \tanh\left(\frac{\theta_i - \theta_{iOC}}{\Delta\theta_{iOC}}\right)\right] \\ & + \frac{1}{2}\left[1 - \left(\frac{\omega}{\Omega_J}\right)_{OM}\right]\left[1 + \tanh\left(\frac{\theta_i - \theta_{iMM}}{\Delta\theta_{iMM}}\right)\right],\end{aligned} \tag{19}$$

where $(\omega/\Omega_J)_{Open}$ is the angular velocity on open field lines, taken to be the *Isbell et al.* [1984] value given by equation (18) for the chosen value of the conductance $\Sigma_P^* = 0.2$ mho and $V_{SW} = 400$ km s^{-1} (giving $(\omega/\Omega_J)_{Open} \approx 0.091$), and $(\omega/\Omega_J)_{OM}$ is the angular velocity in the outer magnetosphere to which the angular velocity in the middle magnetosphere falls at its outer edge, taken to be 0.25 and 0.5 in our two models as discussed above. The position and width of the change in angular velocity across the middle magnetosphere are governed by parameters θ_{iMM} and $\Delta\theta_{iMM}$, respectively. We take these to have the values of 15.5° and 0.4°, respectively, so that the principal change in angular velocity takes place over ~1° of colatitude, between ~15° and ~16°, also in conformity with the above discussion. Similarly, the change in angular velocity between $(\omega/\Omega_J)_{Open}$ and $(\omega/\Omega_J)_{OM}$ across the boundary of open field lines is governed by θ_{iOC} and $\Delta\theta_{iOC}$. The position of the open-closed field line boundary, θ_{iOC}, is chosen such that the amount of open flux enclosed is 500 GWb as above, giving $\theta_{iOC} \approx 10.25°$. With regard to $\Delta\theta_{iOC}$, the open-closed field line boundary itself has zero width, of course, since field lines are either open or closed. However, $\Delta\theta_{iOC}$ actually determines the finite width of the field-aligned current region flowing at the boundary, which, in conformity with our related Saturn model [*Cowley et al.*, 2004a, 2004b] we may reasonably take to be a few hundred kilometers in latitudinal extent. Here therefore we take $\Delta\theta_{iOC} = 0.125°$, such that the width of the boundary region, roughly ~$3\Delta\theta_{iOC}$, is ~450 km at ionospheric heights. With these parameters, the angular velocity models obtained from equation (19) are shown in Figure 1a, plotted from the pole to 20° colatitude. The solid and dashed lines show the models with $(\omega/\Omega_J)_{OM}$ equal to 0.25 and 0.5, respectively. These will be referred to as the "low" and "high" angular velocity models, respectively, in the discussion below, possibly reflecting expanded or compressed magnetospheric conditions as previously mentioned.

[18] In Figure 1b we also show the corresponding profiles of the electrostatic potential $\Phi_i(\theta_i)$ in the inertial frame, obtained by integrating

$$\frac{d\Phi_i}{d\theta_i} = B_i R_i^2 \sin\theta_i\, \omega(\theta_i), \tag{20}$$

where we have taken the arbitrary zero of potential to lie at the pole, $\theta_i = 0°$. The solid and dashed lines again show the potentials for the "low" and "high" angular velocity models, respectively, while the dotted line corresponds to rigid corotation at all colatitudes, for purposes of comparison. Owing to the essentially common angular velocity in

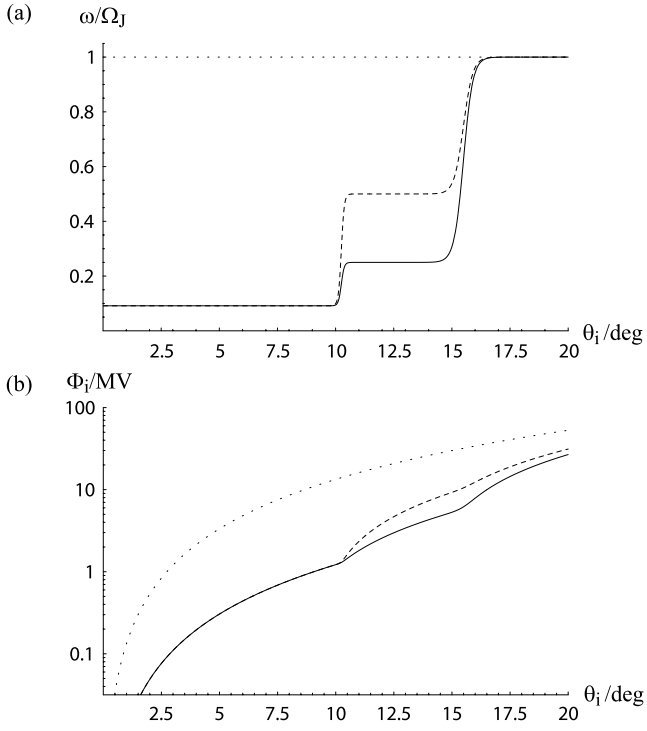

Figure 1. (a) Jupiter plasma angular velocity models employed in this study, normalized to Jupiter's rotational angular velocity Ω_J, plotted versus colatitude θ_i in the ionosphere between the pole and 20°. These are obtained from equation (19), with $(\omega/\Omega_J)_{Open} \approx 0.091$ given by equation (18) with $\Sigma_P^* = 0.2$ mho and $V_{SW} = 400$ km s^{-1}, $(\omega/\Omega_J)_{OM}$ equal to 0.25 (solid line) and 0.5 (dashed line), giving the "low" and "high" angular velocity models, respectively, and $\theta_{iOC} \approx 10.25°$, $\Delta\theta_{iOC} = 0.125°$, $\theta_{iMM} = 15.5°$, and $\Delta\theta_{iMM} = 0.4°$. The horizontal dotted line shows rigid corotation. (b) Corresponding profiles of electrostatic potential in the ionosphere associated with the plasma flow in the inertial frame plotted versus colatitude θ_i, obtained from equation (20). The arbitrary zero of potential has been taken to lie at the pole, $\theta_i = 0°$. The solid and dashed lines again show values for the "low" and "high" angular velocity models, respectively, while the dotted line corresponds to rigid corotation over the whole region for comparison purposes.

the open field region in our two models (Figure 1a), the dashed and solid lines are distinguishable only beyond the open-closed field line boundary at ~10.25°. The voltage thus rises from zero at the pole to ~1.3 MV at the open-closed boundary in both cases, and then to ~6 and ~10 MV in the middle magnetosphere regions of the "low" and "high" angular velocity models, respectively, before increasing to ~27 and ~31 MV, respectively, at the 20° colatitude boundary of the plot. These results for the field-perpendicular voltage will be compared with the field-aligned voltages required by auroral acceleration in section 3.4 below.

3.2. Pedersen Current and Energy Transfer

[19] Given the plasma angular velocity model, we can now use equation (3) to determine the height-integrated Pedersen current intensity, once a value of the effective Pedersen conductance has been chosen. This is not a well-determined parameter, but has been chosen to have the value $\Sigma_P^* = 0.2$ mho for a number of reasons. First, the value is reasonably in line with estimates based on ionospheric models [e.g., *Strobel and Atreya*, 1983]. Second, when employed in self-consistent middle magnetosphere models with realistic Io plasma mass outflow rates, it results in reasonably realistic angular velocity profiles [e.g., *Hill*, 2001; *Cowley and Bunce*, 2002]. Third, when employed in the *Isbell et al.* [1984] formula (equation (18)), it yields "stagnant" flow conditions on open field lines in conformity with the results of *Stallard et al.* [2003]. Fourth, and most definitively with regard to the present model, when combined with the angular velocity models given by equation (19), it yields total Pedersen currents at the poleward boundary of the middle magnetosphere region of ~50 MA per hemisphere, thus implying that the total radial current flowing in the equatorial plane in the outer region of the middle magnetosphere current sheet is ~100 MA. This is in line with Galileo magnetic observations [*Khurana*, 2001; *Nichols and Cowley*, 2004], and ensures that the overall currents flowing in the model are realistic.

[20] Using this value therefore, in Figure 2a we show the height-integrated Pedersen current intensity versus colatitude for the "low" (solid line) and "high" (dashed line) angular velocity models. It can be seen that the current intensity increases near-linearly within the region of open field lines to reach a peak value of ~0.4 A m^{-1} at the boundary. This is due to the near-constant angular velocity of the plasma in this region, such that the actual velocity of the plasma (in the neutral atmosphere rest frame), and hence the electric field and current, increase linearly with distance from the magnetic axis (see equation (3)). Across the open field line boundary the current then drops as the angular velocity increases somewhat toward rigid corotation, more so for the "high" angular velocity model than for the "low" angular velocity model, following which the current rises again due to a corresponding effect in the outer magnetosphere region. Finally, the current intensity falls precipitously to zero across the middle magnetosphere region as the angular velocity of the plasma increases to approach rigid corotation.

[21] Using equations (8) and (9), we can also compute the planetary power per unit area that is transferred by the current system to atmospheric heating and to the magnetosphere. These are shown in Figures 2b and 2c, respectively, plotted versus colatitude on the same vertical scales, so that they may readily be compared. It can be seen that on open field lines the power is fed mainly into atmospheric heating. Integration over the whole open field region yields a total power input to the atmosphere (per hemisphere) of ~200 TW, with ~20 TW being expended in twisting the field in the tail lobe. On closed field lines the distribution is somewhat more even, with ~540 and ~240 TW being dissipated (per hemisphere) in the atmosphere, and ~230 and ~270 TW being transferred to the magnetospheric plasma, in the "low" and "high" angular velocity models, respectively. These relative values directly reflect the angular velocity models, since it is readily seen from equations (8) and (9) that

$$\frac{p_M}{p_A} = \frac{\omega}{(\Omega_J - \omega)}, \tag{21}$$

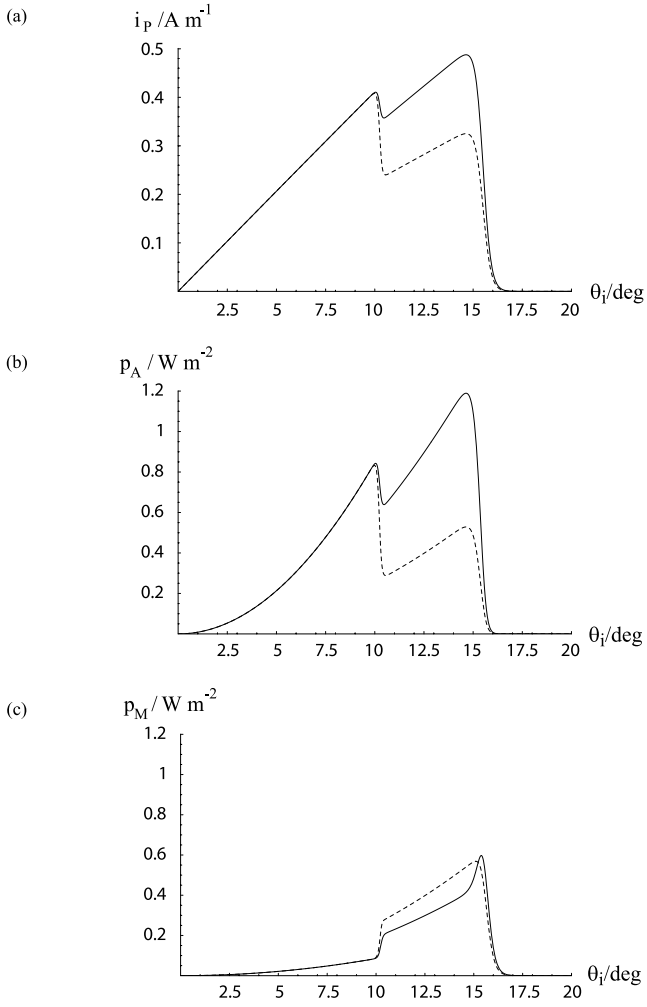

Figure 2. Ionospheric currents and related energy transfers in the constant conductance Jupiter models, showing (a) the height-integrated equatorward Pedersen current intensity obtained from equations (3) and (19) with $\Sigma_P^* = 0.2$ mho, (b) the corresponding power per unit area of ionosphere dissipated from planetary rotation into upper atmosphere heating from equation (9), and (c) the power per unit area of ionosphere transferred from planetary rotation to the magnetosphere from equation (8). As in Figure 1, the solid line shows values for the "low" angular velocity model, while the dashed line shows values for the "high" angular velocity model.

so that most of the power is dissipated in the atmosphere when ω is strongly subcorotational, as in the open field region, while favoring the magnetosphere increasingly as the plasma angular velocity rises toward rigid corotation on closed field lines. Overall, in the "low" angular velocity model ~740 TW is input to the upper atmosphere and ~250 TW to the magnetosphere (per hemisphere), while in the "high" angular velocity model ~440 TW is input to the upper atmosphere and ~290 TW to the magnetosphere. These results are collected and summarized in Table 1. It will be noted that the powers are more than two orders of magnitude higher than the globally averaged input of solar EUV energy into Jupiter's thermosphere (~1 TW) [e.g., *Yelle and Miller*, 2004]. It thus seems reasonable to suppose that atmospheric heating due to magnetosphere-ionosphere coupling may make a significant contribution to a resolution of the issue of why Jupiter's thermosphere is over five times hotter than expected for solar EUV input alone (~940 K observed compared with ~160 K expected [e.g., *Yelle and Miller*, 2004]).

3.3. Total Pedersen Current and Field-Aligned Current

[22] We now consider the variations of the total Pedersen current given by equation (5) and the field-aligned current that is required by its divergence given by equation (6). The total Pedersen current for the two angular velocity models is shown versus colatitude in Figure 3a. It can be seen that the equatorward current grows approximately as the square of the distance from the axis within the open field region, due to the approximately linear growth of the height-integrated current intensity in this region seen in Figure 2a, reaching ~30 MA at the open field line boundary. This requires an approximately uniform downward field-aligned current throughout this region. The total Pedersen current then falls across the open field boundary as the angular velocity rises in the outer magnetosphere, by ~3 MA for the "low" angular velocity model, for which the angular velocity increase is least, and by ~12 MA for the "high" angular velocity model, for which the increase is larger. Field-aligned currents of these magnitudes must therefore flow up the field lines in the boundary region. The Pedersen current then grows again across the outer magnetosphere, requiring downward field-aligned current in this region, before peaking at ~50 and ~35 MA for the "low" and "high" angular velocity models, respectively, at the outer boundary of the middle magnetosphere. The current then falls rapidly to zero as the near-rigid corotation condition is approached across the middle magnetosphere, thus requiring the above peak currents to exit the ionosphere along the field lines across this region.

[23] The field-aligned current profiles derived from equation (6) are then shown in Figure 3b, where positive values represent currents directed upward out of the ionosphere. As anticipated in the above discussion, the currents are directed downward into the ionosphere throughout the open field region and in the outer magnetosphere, with almost constant values of ~0.07 μA m^{-2} in the open field region, and ~0.06

Table 1. Powers Per Hemisphere Transferred From Planetary Rotation to Upper Atmospheric Heating and to the Magnetosphere in the Constant Conductance Models of Section 3

	"Low" Angular Velocity Model	"High" Angular Velocity Model
Power to upper atmosphere, TW		
Open field lines	201	200
Closed field lines	541	242
Total	743	442
Power to magnetosphere, TW		
Open field lines	21	22
Closed field lines	228	272
Total	249	294
Total power, TW		
Open field lines	222	221
Closed field lines	770	514
Total	992	735

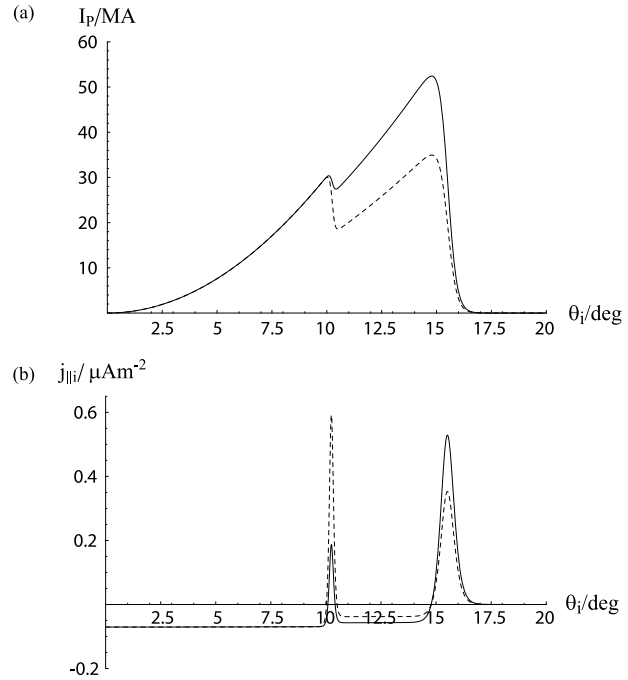

Figure 3. Total current and field-aligned current in the constant conductance Jupiter models, showing (a) the total equatorward Pedersen current obtained from equation (5), and (b) the field-aligned current density just above the ionosphere obtained from equation (6). As in Figure 1, the solid line shows values for the "low" angular velocity model, while the dashed line shows values for the "high" angular velocity model.

and ~0.04 μA m^{-2} in the outer magnetosphere in the "low" and "high" angular velocity regions, respectively. Relatively narrow rings of upward field-aligned current then flow at the open field boundary and in the middle magnetosphere region. With the model parameters chosen, for the "low" angular velocity model the upward current density peaks at ~0.2 μA m^{-2} at the open field boundary and at ~0.5 μA m^{-2} in the middle magnetosphere, while for the "high" angular velocity model the balance is reversed, with the upward current density peaking at ~0.6 μA m^{-2} at the open field boundary and at ~0.4 μA m^{-2} in the middle magnetosphere. The overall latitudinal width of these upward current regions are ~0.4° and ~1.5°, respectively, corresponding to distances of ~450 and ~1800 km at ionospheric heights.

3.4. Auroral Electron Acceleration and Precipitated Energy Flux

[24] We now employ the theoretical results given in section 2.4 above, based on *Knight* [1973], to consider the auroral emissions that are expected to be associated with the regions of upward field-aligned current. These depend not only on the current density values themselves but also on the properties of the magnetospheric electron population that provides the source of the downward precipitating particles. The source parameters employed, and quantities derived from them, are collected together in Table 2. We have used three different source populations, corresponding to the middle magnetosphere, the outer magnetosphere, and the magnetosheath. The latter two are both applied to the upward current flowing at the open field boundary, it being recognized that this current may flow partially on open (magnetosheath) and partially on closed (outer magnetosphere) field lines. For the middle magnetosphere, the electron density N and the thermal energy W_{th} are taken to be 0.01 cm^{-3} and 2.5 keV, respectively, in conformity with the Voyager observations of *Scudder et al.* [1981] and previous modeling studies [e.g., *Cowley et al.*, 2001; *Nichols and Cowley*, 2004]. From equation (13) this gives a limiting current density in the absence of field-aligned acceleration $j_{||i0}$ of ~0.013 μA m^{-2} (Table 2), which we note is much less than the model upward current densities throughout essentially the whole of the middle magnetosphere region, thus implying a general requirement for downward electron acceleration in this region. The unaccelerated precipitating electron energy flux E_{f0} from equation (14) is then ~0.067 mW m^{-2} (Table 2), which corresponds to a sub-kR UV auroral emission (below the ~1 kR sensitivity of existing observational techniques). The corresponding values employed for the outer magnetosphere are 0.02 cm^{-3} and 250 eV, giving a limiting current density and energy flux of ~0.0085 μA m^{-2} and ~0.0042 mW m^{-2}, while for the magnetosheath we employ 0.5 cm^{-3} and 50 eV, giving a limiting current density and energy flux of ~0.095 μA m^{-2} and ~0.0095 mW m^{-2}. These values are based on the Ulysses thermal electron data presented by *Phillips et al.* [1993a, 1993b], as employed in previous modeling studies of the Jovian cusp by *Bunce et al.* [2004]. We note that the limiting currents of both plasma components are less than the peak upward currents at the open field boundary for both models, thus also implying electron acceleration in all cases, though only marginally so for magnetosheath electrons in the "low" angular velocity model. We also note that the unaccelerated energy fluxes in both cases are less than those deduced for the middle magnetosphere source and hence would also not give rise to detectable UV emissions.

[25] Results are shown in Figure 4, where the upper, middle, and lower panels show the minimum accelerating voltages obtained from equation (15), the minimum radial distances of the acceleration region from equation (16), and the precipitating energy fluxes of accelerated particles, respectively. In each case we focus on a restricted range of

Table 2. Properties of the Magnetospheric Source Electron Parameters Employed in Auroral Calculations

	Magnetosheath Source	Outer Magnetosphere Source	Middle Magnetosphere Source
Electron density N, cm^{-3}	0.5	0.02	0.01
Electron thermal energy W_{th}, keV	0.05	0.25	2.5
Unaccelerated current density $j_{\|\|i0}$, μA m^{-2}	0.095	0.0085	0.013
Unaccelerated energy flux E_{f0}, mW m^{-2}	0.0095	0.0042	0.067

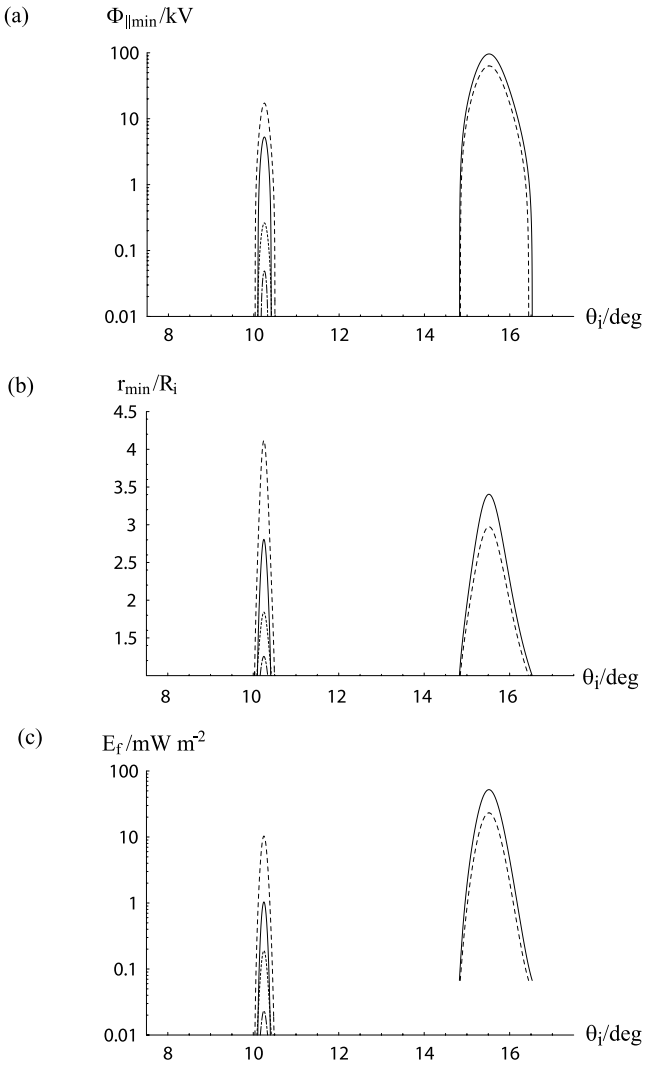

Figure 4. Auroral parameters for the constant conductance Jupiter models, based on the field-aligned current density profiles shown in Figure 3 (specifically in regions of upward field-aligned current), and the magnetospheric source electron parameters given in Table 2. The panels show (a) the minimum value of the field-aligned accelerating voltage given by equation (15), (b) the minimum radial distance of the acceleration region, normalized to the ionospheric radial distance R_i, given by equation (16), and (c) the precipitating electron energy flux given by equation (17). The plot shows the colatitude range containing the regions of upward directed field-aligned current, between 7.5° and 17.5°. As in previous figures, the solid line shows values for the "low" angular velocity model, while the dashed line shows values for the "high" angular velocity model, specifically assuming the outer magnetosphere source parameters in the vicinity of the open-closed field line boundary near ~10.25°. Values for the magnetosheath source parameters are shown by the dot-dashed and dotted lines for the "low" and "high" angular velocity models, respectively.

colatitudes within which the upward currents flow, between 7.5° and 17.5°. The format of the plots follows that employed previously, where solid and dashed lines show values for the "low" and "high" angular velocity models, respectively, specifically for the outer magnetosphere source plasma at the open-closed field boundary. Corresponding results for the magnetosheath source plasma are shown by the dot-dashed line for the "low" angular velocity model and by the dotted line for the "high" angular velocity model.

[26] If we examine the middle magnetosphere region first, it can be seen from Figure 4a that minimum accelerating voltages peak at ~100 and ~60 kV for the "low" and "high" angular velocity models, respectively, thus implying precipitating energetic primary electron beams at essentially these energies. Such auroral electron energies are entirely comparable with those deduced from main oval UV spectra by *Gustin et al.* [2004]. We note from Figure 1b that such field-aligned voltages correspond to values which are only ~1% of the field-perpendicular voltage between the pole and the middle magnetosphere, thus implying only small poleward displacements of the electric equipotentials across the field lines in the auroral acceleration region [see also *Cowley and Bunce*, 2001; *Nichols and Cowley*, 2005]. The corresponding energy fluxes in Figure 4c peak at ~50 and ~20 mW m^{-2}, respectively, associated with unabsorbed UV auroral emissions of ~500 and ~200 kR. According to the discussion in section 2.4, hydrocarbon absorption will then reduce these values by factors of 2–3, to ~200 and ~100 kR, respectively, at the primary electron energies involved. The observed brightness of the main oval typically varies between ~50 and ~300 kR [e.g., *Grodent et al.*, 2003a; *Gustin et al.*, 2004], these values thus being vary comparable with those deduced here. The total power input to the Jovian atmosphere associated with this precipitation can also be derived by integrating the energy flux over the whole middle magnetosphere region. The powers obtained are ~3.6 and ~1.6 TW per hemisphere for the "low" and "high" angular velocity models, respectively, thus again being comparable to typical values deduced from auroral observations [e.g., *Grodent et al.*, 2003a, 2003b; *Clarke et al.*, 2004]. Overall therefore it seems reasonable to conclude that the precipitation characteristics in the middle magnetosphere region in the model are compatible with observations of the Jovian main oval emissions, in conformity with previous conclusions [e.g., *Cowley and Bunce*, 2001; *Cowley et al.*, 2002, 2003a; *Nichols and Cowley*, 2004]. Figure 4b also shows that the minimum radial distance of the acceleration region is ~3–3.5 R_J in both models, such that the accelerated primary electron beams may form the source of cyclotron emissions underneath the acceleration region at frequencies ~1–30 MHz, corresponding mainly to "non-Io-DAM" radio emissions (see, e.g., the review by *Clarke et al.* [2004]).

[27] Our model shows, however, that Jovian auroral emissions may also occur at smaller colatitudes, associated with the open-closed field line boundary. Using the outer magnetosphere electron source, the minimum accelerating voltages peak at ~5 and ~15 kV for the "low" and "high" angular velocity models, with peak energy fluxes of ~1 and ~10 mW m^{-2}, respectively. These field-aligned voltages again correspond to ~1% of the voltage drop between the

Table 3. Total Powers Per Hemisphere of Precipitating Accelerated Electrons Integrated Over the Upward Field-Aligned Current Regions of the Constant Conductance Models of Section 3[a]

Precipitating Auroral Electron Powers, GW	"Low" Angular Velocity Model	"High" Angular Velocity Model
Middle magnetosphere	3550	1580
Open field boundary (outer magnetosphere source)	12.2	141
Open field boundary (magnetosheath source)	0.27	2.65

[a]Values are provided for the middle magnetosphere and the open field boundary region. The latter values assume that the whole of the current at the boundary is carried either by outer magnetosphere electrons or magnetosheath electrons in each case.

pole and the open-closed field line boundary (Figure 1b), thus again implying only very small cross-field displacements of the electric equipotentials. The energy fluxes correspond to UV auroral intensities of ~10 and ~100 kR, respectively, and hence to auroras which, while being clearly observable, are generally less bright than those of the main oval (the effect of hydrocarbon absorption at ~10 keV primary electron energies being small according to the discussion in section 2.4). Although the currents flowing in the open field boundary are comparable to those of the middle magnetosphere region in our model, and hence so are the precipitating electron number fluxes, the mean energy of the accelerated electrons, ~10 keV, is significantly less than for the middle magnetosphere, ~100 keV, due to the lower temperature of the magnetospheric electron source population (Table 2). Thus the total precipitating electron power integrated over the whole boundary region is also significantly less, being ~10 and ~140 GW (per hemisphere) for the "low" and "high" angular velocity models, respectively, assuming that the whole of the current is carried by outer magnetosphere electrons. The values are even smaller assuming the cool dense magnetosheath source, with accelerating voltages from a few tens to a few hundred volts, and energy fluxes from a few tenths to a few hundredths of a mW m^{-2}. The total precipitating electron powers in this case are ~0.3 and ~3 GW (per hemisphere) for the "low" and "high" angular velocity models, again assuming that the whole of the current is carried by magnetosheath electrons. These total precipitating electron power values are also collected together in Table 3. In general, however, we may suppose that part of the boundary current will be carried by outer magnetosphere electrons (some lower-latitude portion), and part by magnetosheath electrons (some higher-latitude portion). In this case, the emission at the boundary will generally be dominated by that fraction at lower latitudes which is carried by outer magnetosphere electrons.

[28] Overall, the results show that while our model is certainly consistent with the appearance of discrete auroral emissions associated with the open-closed field line boundary at high latitudes, the Jovian auroral emissions will be dominated by those associated with the middle magnetosphere. The difference between the auroral powers in the two regions is the most marked for our "low" angular velocity model, possibly representing an expanded magnetosphere, in which the increase in plasma angular velocity at the open field line boundary is much less than that across the middle magnetosphere (Figure 1a). However, for our "high" angular velocity model, possibly representing a more compressed magnetosphere, the change in angular velocity across the open field boundary is increased, while that across the middle magnetosphere region is reduced, such that the changes across the two regions become comparable. This has the effect of reducing the accelerating voltages and auroral emissions in the middle magnetosphere region, in conformity with the general conclusions of *Cowley and Bunce* [2003a], while increasing them in the open field boundary region. With regard to observations, the power of the Jovian auroras observed poleward of the main oval is indeed found to be much smaller than that of the main oval, in conformity with the above general conclusions. Quantitatively, however, the polar UV power is found to correspond to an electron energy input per hemisphere of ~500 GW, ~20% of the main oval energy input [e.g., *Grodent et al.*, 2003b], which is considerably larger than the model estimates made above (~10 and ~140 GW). Perhaps not surprisingly therefore our simple axisymmetric model appears to provide only a partial explanation of the auroral precipitation observed poleward of the main oval. The most likely component which may correspond to our currents at the open field boundary are the most poleward emissions that border the aurorally dark region on their poleward side [*Pallier and Prangé*, 2001, 2004]. Preliminary analyses of these emissions indeed indicate that they are due to precipitating electrons of ~10 keV energy, with typical intensities of order tens of kR, very comparable to the theoretical estimates made above. However, these observations also show that in addition to localized features such as the "cusp spot" which clearly cannot be described by our simple axisymmetric model, significant structured emissions are also often present in the region between these most poleward emissions and the main oval. These have no direct counterpart in the present model, thus suggesting the possible presence of additional flow structures that are not represented in our "outer magnetosphere" region and whose physical origins are at present unclear. We also note that the precipitating electron powers estimated here apply only to the accelerated electron component in discrete auroras associated with regions of upward field-aligned current. In addition to this, widespread "diffuse" electron precipitation will also generally be present in the closed field region, due to pitch-angle scattering of the hot trapped magnetospheric particle populations. Judging from the unaccelerated energy fluxes of the electron populations in Table 1, however, only low-level energy fluxes and UV emissions are expected from this source.

4. Jupiter Model With Variable Conductance

[29] Ionospheric modeling results presented by *Millward et al.* [2002] have shown that energetic electron precipitation into the Jovian ionosphere at the currents (electron number fluxes) envisaged here can significantly enhance the ionospheric Pedersen conductance above the "background"

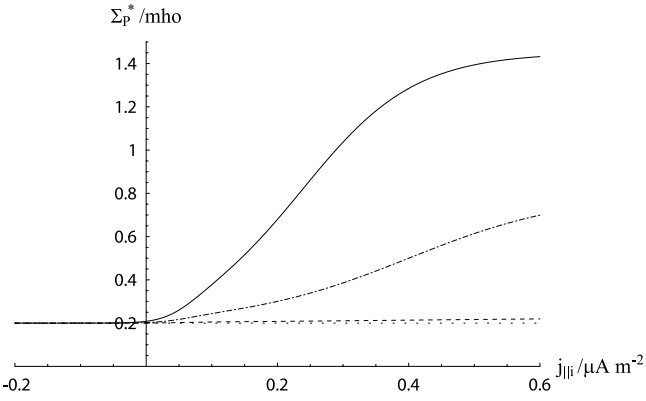

Figure 5. Model variations of the effective height-integrated ionospheric Pedersen conductance on field-aligned current density for the three magnetospheric source populations employed, whose parameters are given in Table 2. These are based on equation (22), with parameter values given in the text. The solid line is for the middle magnetosphere, the dot-dashed line for the outer magnetosphere, and the dashed line for the magnetosheath source on open field lines. The lowest dotted line shows the constant background conductance of 0.2 mho to which these curves are asymptotic for negative (downward) currents.

levels considered in section 2. Electrons with energy ~60 keV were found to be particularly effective, since they deposit their energy and create ionization directly within the Pedersen layer. A beam of such electrons with a number flux equivalent to a field-aligned current of 1 μA m^{-2} was found to increase the Pedersen conductance to ~7.5 mho, a value much larger than the value of 0.2 mho employed in section 2. Conductance (or effective conductance) values are reduced, however, for lesser currents (as is generally the case in our solutions), higher or lower electron energies, and by neutral atmosphere drag. *Nichols and Cowley* [2004] self-consistently incorporated precipitation feedback on conductance in their model of Jupiter's middle magnetosphere, using a simple relation between field-aligned current and conductance based on *Millward et al.*'s [2002] results. They found that significant quantitative effects were produced relative to constant conductance models, with the upward field-aligned current becoming concentrated in the inner part of the middle magnetosphere, mapping in the equatorial plane to radial distances ~20 R_J. Such a concentration is in agreement with the experimental results of *Khurana* [2001] derived from Galileo magnetic field data. It is therefore of interest to examine the effects of precipitation-induced conductance variations in the present model. The calculation is not fully self-consistent like that of *Nichols and Cowley* [2004], however, since the plasma angular velocity profile will be prescribed in the same way as in section 3 above, but the calculation can be applied to the whole polar ionosphere rather than just to the middle magnetosphere region. Insight can thus be gained on how the overall field-aligned current structures will be modified when the conductance is locally enhanced within regions of upward field-aligned current.

[30] As indicated above, the conductance enhancements produced by precipitation depend not only on the electron current (number flux) but also on the electron energy. The electron energy in turn depends on the magnetospheric source population, which determines the acceleration voltage through equation (15). Here we employ the same three source populations as given in Table 2, corresponding to the magnetosheath (open field lines), the outer magnetosphere, and the middle magnetosphere, and have determined how the conductance depends on the field-aligned current for each of these sources using the same approach as that of *Nichols and Cowley* [2004]. Briefly, for a given magnetospheric source, the accelerating voltage and precipitating energy flux are determined for a given current density by equations (15) and (17). As the accelerated electrons travel down the field lines to the ionosphere, the distribution is assumed to be spread in energy about the characteristic energy determined by the accelerating voltage, both to higher and lower energies, though preserving the number flux and the energy flux. Using simple power-law assumptions about the form of the distribution, the precipitating number flux in various electron energy bands are then calculated and used to determine the contributions to the Pedersen conductance from the results presented by *Millward et al.* [2002] (see *Nichols and Cowley* [2004] for further details). These contributions are then summed to determine the total enhancement of the Pedersen conductance from the full precipitating accelerated (but spread) electron distribution. This procedure is repeated for various precipitating current densities to determine how the conductance enhancement depends on the current for that magnetospheric source population. The enhancement of the effective conductance is then taken to be just half this value, assuming $k \approx 0.5$ in equation (4) on the basis of the results of *Millward et al.* [2005]. Finally, we represent these numerically generated models by a simple function of the current density which has the same form (but differing coefficients) for each source population. Specifically, conductance dependence on the current has been taken to have the form

$$\Sigma_P^*(j_{\|i}) = \Sigma_{P0}^* + \Delta\Sigma_P^* \left[\frac{1}{2}\left(1 + \tanh\left(\frac{j_{\|i} - j_{\|i}^*}{\Delta j_{\|i}^*}\right)\right)\right] \cdot \left[\frac{1}{2}\left(1 + \tanh\left(\frac{j_{\|i} - j_{\|i}^0}{\Delta j_{\|i}^0}\right)\right)\right], \quad (22)$$

where $\Sigma_{P0}^* = 0.2$ mho is the constant background conductance, as employed in sections 2 and 3, and the second term describes the electron source-dependent enhancement due to precipitation. For the middle magnetosphere we employ $\Delta\Sigma_P^* = 1.25$ mho, $j_{\|i}^* = 0.24$ μAm^{-2}, and $\Delta j_{\|i}^* = 0.17$ μAm^{-2}, for the outer magnetosphere $\Delta\Sigma_P^* = 0.6$ mho, $j_{\|i}^* = 0.4$ μAm^{-2}, and $\Delta j_{\|i}^* = 0.25$ μAm^{-2}, while for the magnetosheath we take $\Delta\Sigma_P^* = 0.0275$ mho, $j_{\|i}^* = 0.4$ μAm^{-2}, and $\Delta j_{\|i}^* = 0.45$ μAm^{-2}. We also take $j_{\|i}^0 = \Delta j_{\|i}^0 = 0.05$ μAm^{-2} in the final term in equation (22), which is used to ensure that the model conductance enhancement reduces rapidly to small values for downward (negative) field-aligned currents. With these values, the variation of the effective Pedersen conductance with field-aligned current for each of the three source populations is shown in Figure 5, for currents up to 0.6 μA m^{-2} (the approximate limit of validity of the above formulas). The solid line shows the

variation for the middle magnetosphere source, the dot-dashed line for the outer magnetosphere source, and the dashed line for the magnetosheath source. The lowest dotted line shows the background conductance of 0.2 mho to which these models are asymptotic for negative field-aligned current. It can be seen that for the current densities of interest here, up to several tenths of a μA m^{-2}, the increases in the conductance for the low-density relatively energetic middle magnetosphere source are very high (more than a factor of $\sim$5), are more modest for the cooler outer magnetosphere source (factors of $\sim$2–3), and are essentially negligible for the cold dense magnetosheath source.

[31] For purposes of numerical calculation, equation (22) has been applied with coefficients $\Delta\Sigma_P^*$, $j_{\|i}^*$, and $\Delta j_{\|i}^*$ varying continuously with latitude between the values quoted above. That is, using a hyperbolic tangent function of colatitude, we have switched continuously from magnetosheath coefficients to outer magnetosphere coefficients in a narrow region about the open-closed field line boundary, and from outer magnetosphere to middle magnetosphere coefficients in the interface between the latter regions. Specifically, the width of the transition region at the open-closed field line boundary in the results to be presented below is taken to be $\sim$0.05°, small compared with the width of the current sheet at that boundary of $\sim$0.25°, while the transition between the outer and middle magnetosphere is centered at 14°, and is taken to be $\sim$1° wide. With these transitions in coefficients, then, the effective Pedersen conductance becomes an explicit continuous function of $j_{\|i}$ and θ_i. Substitution of equations (3) and (5) into (6), and retaining the conductance within the differential, then yields the following nonlinear first-order equation for $j_{\|i}$

$$B_i\Omega_J \frac{d}{d\theta_i}\left[\sin^2\theta_i\left(1-\frac{\omega(\theta_i)}{\Omega_J}\right)\Sigma_P^*\left(j_{\|i},\theta_i\right)\right]+\sin\theta_i\, j_{\|i}=0, \quad (23)$$

where $(\omega(\theta_i)/\Omega_J)$ is given by equation (21). This equation is solved numerically with the use of one boundary condition. Here we have started the solution close to the pole $\theta_i = 0°$ with a (negative) current density equal to that of the constant conductance solution, though the solutions elsewhere are not sensitive to this choice. Having found the field-aligned current from the solution of equation (23), and hence the conductance profile, the ionospheric currents follow from equations (3) and (5), the energy transfers from equations (8) and (9), and the auroral parameters from equations (15)–(17). In Figures 6–8 we show results specifically for the Jovian "high" angular velocity model of section 3 (see Figure 1a), where the solid lines show results for the variable conductance calculation, while the dashed lines show the constant conductance (0.2 mho) solution of section 3 for easy comparison. The plots follow the format of Figures 2–4, except that in Figure 7 we also include a plot of the variation of the ionospheric Pedersen conductance with latitude. In the auroral parameter plots in Figure 8 we also only show values derived using magnetosheath source parameters poleward of the boundary of open field lines, and only values derived using outer magnetosphere source parameters equatorward of the boundary, in conformity with the assumptions made above concerning the behavior of the conductance model. Results for the "low" angular velocity model show related features and will not be shown here.

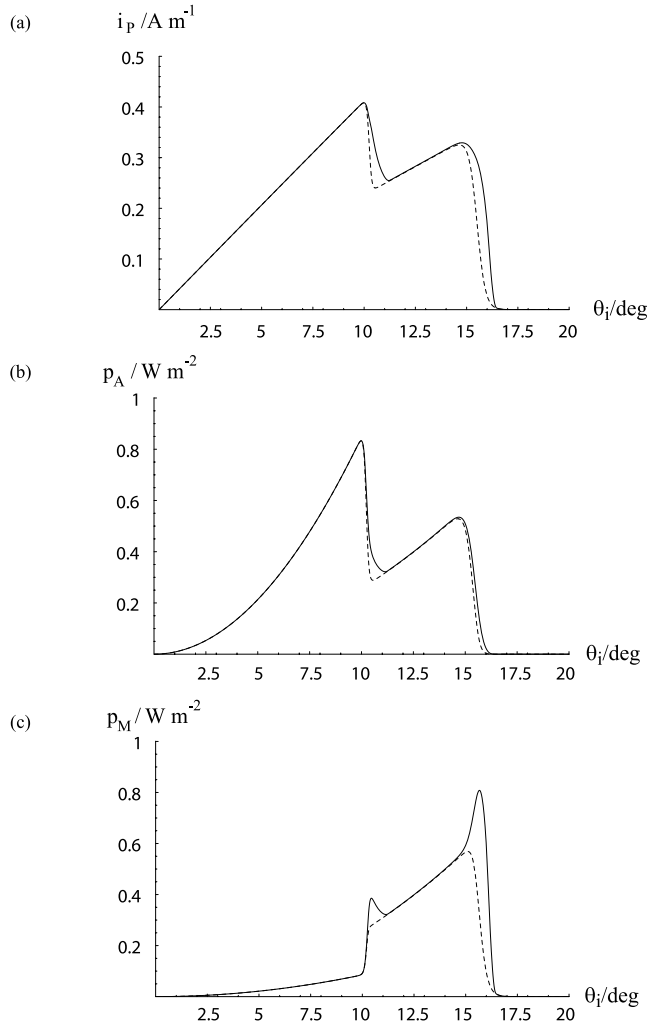

Figure 6. Solutions of the variable conductance problem for the Jupiter "high" angular velocity model (solid lines), in which the ionospheric Pedersen conductance is enhanced in regions of upward field-aligned current by precipitating accelerated magnetospheric electrons. The dashed lines show the constant conductance (0.2 mho) solutions, as also shown by the dashed lines in Figure 2. The plots show (a) the height-integrated equatorward Pedersen current intensity, (b) the corresponding power per unit area of ionosphere input from planetary rotation into upper atmospheric heating, and (c) the power per unit area of ionosphere transferred to the magnetosphere.

[32] First, it can be seen that the overall nature of the solutions is similar to that of the constant conductance solution, being significantly modified only in the layers of upward field-aligned current at the boundary of open field lines and in the middle magnetosphere region. If we first consider the boundary of open field lines near $\theta_i \sim 10°$, it can be seen in Figure 7c that the ionospheric conductance becomes modestly enhanced by precipitation on the equatorward side of the boundary where outer magnetospheric electrons are assumed to carry the current, and that this has the effect of enhancing and maintaining the Pedersen current as the angular velocity increases nearer to rigid corotation. Consequently, the Pedersen current falls less

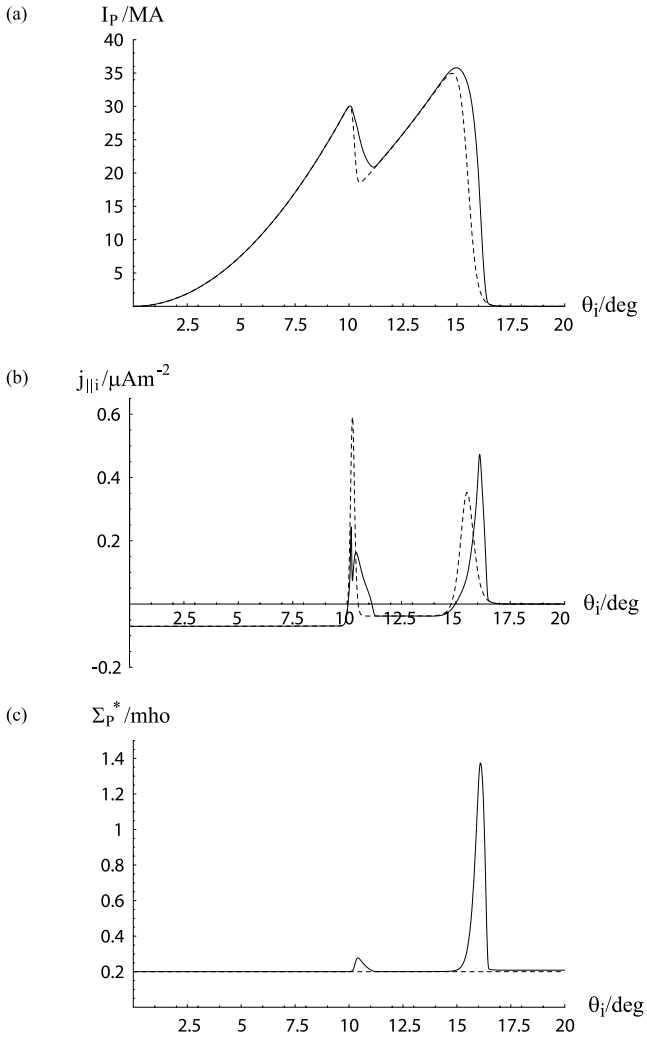

Figure 7. Solutions of the variable conductance problem for the Jupiter "high" angular velocity model (solid lines) showing (a) the total equatorward Pedersen current, (b) the field-aligned current density just above the ionosphere, and (c) the corresponding effective ionospheric Pedersen conductance. The dashed lines show the constant conductance (0.2 mho) solutions, as also shown by the dashed lines in Figure 3.

rapidly with increasing latitude on the equatorward side of the boundary than in the constant conductance solution (Figure 6a), such that the upward current is spread over a wider latitudinal region (~1° overall) and the current density reduced (Figure 7b). The total current flowing up the field lines in the boundary region is also modestly reduced by this effect (Figure 7a), from ~12 to ~9 MA. A further consequence for the auroral parameters is that the accelerating voltages are also reduced due to the reduced current densities, though they are spread over a wider region. However, since the energy flux goes as the square of the current density (equation (17)), the total precipitating electron power is overall reduced. It can be seen in Figure 8a that the peak accelerating voltage on the equatorward side of the boundary is reduced from ~15 to ~4 kV, such that the peak energy flux is strongly reduced from ~10 to ~0.75 mW m^{-2} (Figure 8c). The latter corresponds to a relatively weak UV auroral emission of ~7.5 kR, compared with a ~100 kR peak for the constant conductance model. Overall, integrating over only closed field lines equatorward of the boundary, the total power of precipitating accelerated outer magnetospheric electrons in the vicinity of the boundary is found to be ~24 GW (per hemisphere), compared with ~74 GW for the constant conductance model (this value being about half that given in Table 3 where the

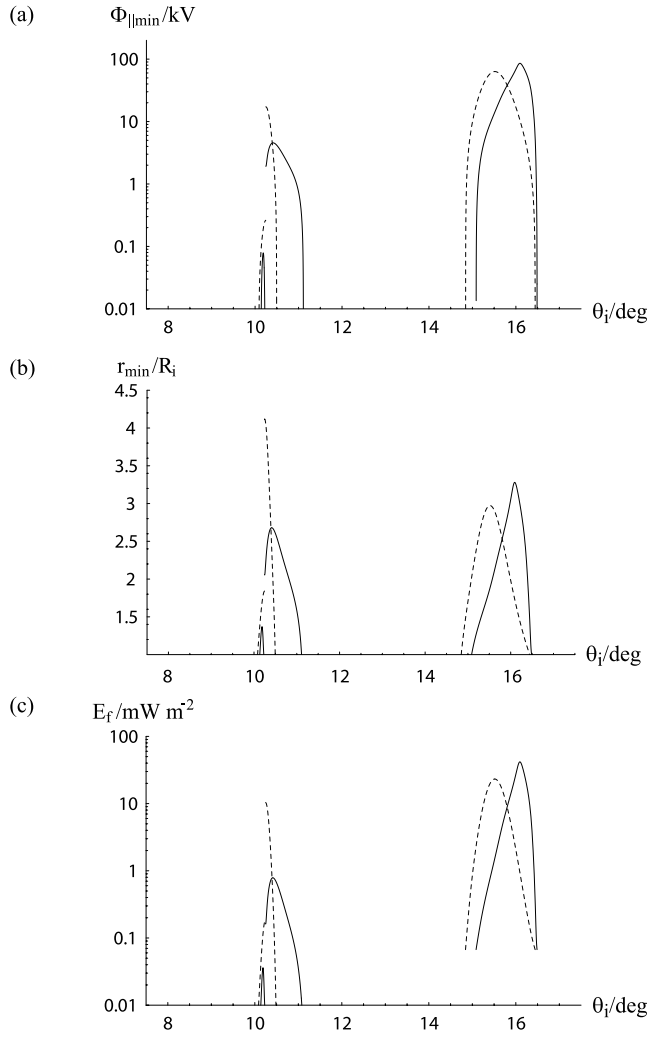

Figure 8. Solutions of the variable conductance problem for the Jupiter "high" angular velocity model (solid lines) showing (a) the minimum value of the field-aligned accelerating voltage in regions of upward field-aligned current, (b) the minimum radial distance of the acceleration region normalized to the ionospheric radial distance R_i, and (c) the precipitating electron energy flux, all on a reduced latitude scale as in Figure 4. The dashed lines show the constant conductance (0.2 mho) solutions, as in Figure 4. Unlike Figure 4, however, values using magnetosheath source parameters are shown (by solid and dashed lines) only on the poleward side of the open field boundary, while values using outer magnetosphere parameters are shown (also by solid and dashed lines) only on the equatorward side of the open field boundary, in conformity with the assumptions made in constructing the conductance variation model.

integral was applied to the whole of the upward current region). The effect of the conductance enhancement at the open field boundary is thus to spread (and somewhat reduce) the upward current and hence to reduce both the energy flux and total power of the precipitating accelerated outer magnetosphere electrons. The power of the precipitating accelerated magnetosheath electrons poleward of the boundary is also sharply reduced from ~1.3 to ~0.2 GW, but this is relatively small in either case.

[33] Turning now to the middle magnetosphere region at the equatorward boundary of the subcorotating plasma, the effect of the conductance enhancement in the region of upward field-aligned current is basically similar to that at the open field boundary, but its consequences for auroral effects are different. That is, as the angular velocity starts to increase toward rigid corotation in the poleward region of the layer, the conductance starts to rise rapidly (Figure 7c), thus tending to maintain the Pedersen current in the layer (Figures 6a and 7a). However, in this case, the rise of the plasma angular velocity continues inexorably, such that the Pedersen current does then fall as the angular velocity approaches rigid corotation. The overall effect is thus to concentrate the upward field-aligned current in a layer on the equatorward side of the middle magnetosphere region, where the field-aligned current densities are enhanced compared with the constant conductance solution (Figure 7b). The auroral parameters are also consequently concentrated and enhanced on the equatorward side of the middle magnetosphere region (Figure 8), with peak energy fluxes doubling from ~20 to ~40 mW m^{-2}. The overall power per hemisphere of precipitating accelerated electrons is also somewhat increased, from ~1.6 TW (as given in Table 3) to ~1.9 TW.

[34] Overall, the effect of the conductance enhancements in regions of upward field-aligned current is to spread the current on the equatorward side of the open field line boundary, thus spreading and reducing the auroral precipitation, while concentrating the current in the equatorward part of the middle magnetosphere region, thus concentrating and enhancing the auroral precipitation in this region. The latter effect therefore mirrors the current concentration effect into the inner part of the middle magnetosphere in the self-consistent calculations presented by *Nichols and Cowley* [2004]. The effect on the planetary rotation powers transferred to atmospheric heating and the magnetosphere are shown in Figures 6b and 6c, respectively. The enhancements of the Pedersen current in regions of upward field-aligned current on closed field lines marginally increases the atmospheric heating effect (Figure 6b), while more strongly enhancing the energy transfer to the magnetosphere (Figure 6c) in those regions. Integrating over the whole polar ionosphere, the power dissipated per hemisphere to atmospheric heating is marginally increased from ~440 TW in the constant conductance solution (see Table 1) to ~460 TW in the variable conductance model. The power transferred to the magnetosphere, however, is more significantly increased from ~290 to ~350 TW per hemisphere.

5. Summary

[35] In this paper we have developed a simple axisymmetric model of the flow and currents in Jupiter's polar ionosphere. This is of a similar nature to the Saturn model presented previously by *Cowley et al.* [2004b], in which the plasma angular velocity is specified at the outset using a combination of observations, previous modeling, and theory, from which the currents and related auroral parameters are then calculated. The plasma angular velocity model incorporates a simple description of four regions mapping to the inner, middle, and outer magnetosphere regions on closed field lines, and the open field region mapping to the tail. In this context the inner magnetosphere is the region where the plasma near-rigidly corotates with the planet, extending to ~20 R_J in the equatorial plane. The plasma angular velocity then falls to some fraction of rigid corotation across the middle magnetosphere, before plateauing at that value in the outer magnetosphere. The fraction concerned is taken to be either a quarter or a half of rigid corotation in the results displayed, the former value corresponding possibly to a more expanded magnetosphere with lower angular velocities on closed field lines and the latter corresponding to a more compressed magnetosphere with higher angular velocities. The open field region is similarly taken to be a region where the flow is strongly subcorotational (~10% of rigid corotation). We have then computed the field-perpendicular and field-aligned current systems implied by the angular velocity model, first assuming a constant value of the effective height-integrated ionospheric Pedersen conductance of 0.2 mho, this value being found to provide overall currents in agreement with observations. From these results we have then been able to discuss three principal issues, concerning overall closure of the current system, the power dissipated to heat in the upper atmosphere and transferred to the magnetosphere, and expectations on auroral emissions associated with electron acceleration above regions of upward field-aligned current.

[36] On the first of these topics, we find in common with previous analyses that the field-aligned current is directed uniformly upward out of the ionosphere in the middle magnetosphere region where the angular velocity falls with increasing latitude. These currents total ~35 and ~50 MA per hemisphere in the two plasma angular velocity models evaluated here. As shown by the dashed lines in Figure 9, these currents then flow radially outward across the field in the equatorial middle magnetosphere, imparting planetary rotational energy and angular momentum to the outwardly diffusing plasma. Part of the current (roughly half in these models) then flows down the field lines again in the outer magnetosphere (certainly on the dayside), while part also flows out to the magnetopause. There it is joined by the smaller upward current (several MA) from the open field boundary region and then flows along the magnetopause to the tail. These tailward directed currents then close through the central region of the twisted tail lobe back to the polar ionosphere to complete the current circuit.

[37] With regard to energy transfers, we find that the total power dissipated from planetary rotation to upper atmospheric heating via the current system is several hundred TW per hemisphere (~400 and ~700 TW per hemisphere in our two models). This compares with a globally averaged solar EUV input to the upper atmosphere of ~1 TW. It thus seems reasonable to suppose that these powers provide an important contribution to resolving the issue of the unexpectedly high temperatures found in the Jovian thermo-

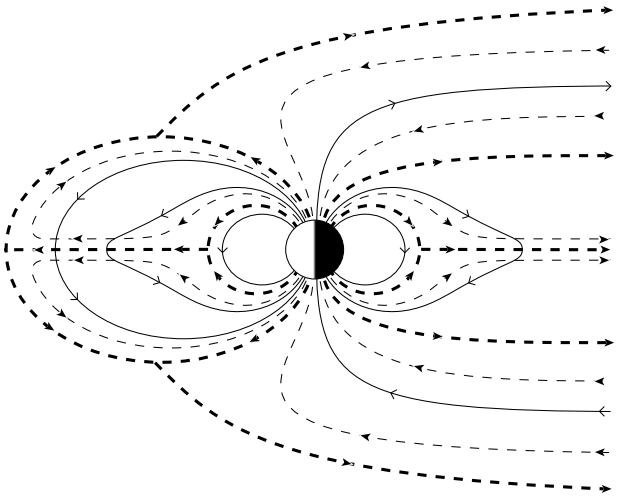

Figure 9. Sketch of the magnetosphere-ionosphere coupling current system in the Jovian magnetosphere in a cross section through the noon-midnight meridian, as implied by the model developed here. The solid lines with arrows represent magnetic field lines, while the dashed lines with arrows represent the direction of current flow. The Sun is to the left in this diagram, and north is upward.

sphere, though the issue remains open of how this power can be globally redistributed from the polar region where it is deposited. The power transferred to the magnetosphere by the current system is found to be ~300 TW in the two models, most of which occurs on closed field lines.

[38] On the topic of discrete auroras produced by field-aligned accelerated electrons, we noted above that the model contains two rings of upward field-aligned current, one occurring at the boundary of open field lines, the other at the equatorward boundary of the region of subcorotating flow mapping to the middle magnetosphere. The field-aligned current densities in the model are comparable in these two regions, peaking at a few tenths of a μA m^{-2} (compared with ~0.05 μA m^{-2} in the downward current regions in the outer magnetosphere and open field region), resulting from the fact that though the total current carried in the middle magnetosphere is significantly larger than at the open field boundary, it is also significantly wider in latitude. These upward current densities require field-aligned acceleration of magnetospheric electrons in all cases, whether carried by magnetosheath or outer magnetosphere electrons at the open field boundary or by hot tenuous electrons in the middle magnetosphere. Discrete auroras are thus expected in both regions, though being dominated in terms of total precipitating electron power by the middle magnetosphere. The total power deposited by precipitating accelerated ~50–100 keV electrons in the middle magnetosphere region is found to be ~2–4 TW per hemisphere, the higher value corresponding to the lower angular velocity model possibly representing a more expanded magnetosphere. These values are comparable to the electron input powers deduced from auroral observations, and are at least two orders of magnitude less than the "Joule heating" values quoted above. The total power deposited by ~5–10 keV electrons in the open field boundary region (~10–150 GW) is then estimated to be one to two orders of magnitude less than for the middle magnetosphere, with the higher value now corresponding to the higher angular velocity model possibly representing a more compressed magnetosphere. These values are somewhat smaller than the ~500 GW deduced from auroral observations poleward of the main oval, such that our model provides only a partial explanation of these emissions. These precipitating discrete auroral electron powers do not include, of course, the possibility of further significant electron energy input to the atmosphere from broadly distributed "diffuse" electron precipitation, due to electron pitch-angle scattering from the trapped hot populations on closed field lines.

[39] It is of interest briefly to compare these results with those obtained from the related Saturn model described previously by *Cowley et al.* [2004b]. In this case the radial distance of the ionosphere is similar to Jupiter, as are the planetary and plasma angular velocities. However, the ionospheric magnetic field strength is a factor of ~20 smaller at Saturn, while the estimated effective Pedersen conductivity is ~5 times larger. These factors then combine to produce ionospheric currents which are overall a factor of ~5 times smaller at Saturn than at Jupiter, while the powers transferred to upper atmospheric heating and to the magnetosphere are around two orders of magnitude less (~4 and ~8 TW, respectively). The Saturn model also produces two rings of upward field-aligned current, one associated with the open-closed field line boundary and the other with the middle magnetosphere, as in the Jupiter model presented here. In the Saturn model, however, the current densities are very asymmetrical, with the current density in the ring at the open field boundary being comparable to that in our Jupiter model, a few tenths of a μA m^{-2}, while that mapping to the middle magnetosphere is much less, ~10 nA m^{-2}, due to the broad region of the ionosphere to which it maps. Consequently, field-aligned acceleration of magnetospheric electrons is required only at the open field boundary in this case, and not in the middle magnetosphere, such that discrete auroras will be dominated by the solar wind interaction. Again, this does not preclude the possibility of additional broadly distributed diffuse electron precipitation from hot trapped magnetospheric electrons on closed field lines.

[40] Finally, we have also presented a development of the Jupiter model in which precipitation-induced modification of the ionospheric conductance is included in the current continuity description, based on the modeling results of *Millward et al.* [2002]. We have shown that this has the effect of spreading the upward field-aligned current on closed field lines at the open field boundary, thereby reducing both the energy flux and the total power of precipitating accelerated outer magnetosphere electrons. In the middle magnetosphere, however, it has the effect of concentrating the upward field-aligned current in the equatorward region of the middle magnetosphere (in agreement with the effect found previously by *Nichols and Cowley* [2004]), thus somewhat increasing both the electron energy flux in this region and the total precipitating electron power.

[41] **Acknowledgments.** This work was partly funded by INTAS grant 03-51-3922. Work at Leicester was also supported by PPARC grant PPA/G/O/2003/00013. EJB was supported by PPARC Postdoctoral Fellowship PPA/P/S/2002/00168. Work at INP Moscow was supported by the RFBR grants 04-05-64396 and 05-05-64435.

[42] Arthur Richmond thanks Vytenis M. Vasyliunas and another reviewer for their assistance in evaluating this paper.

References

Acuña, M. H., K. W. Behannon, and J. E. P. Connerney (1983), Jupiter's magnetic field and magnetosphere, in *Physics of the Jovian Magnetosphere*, edited by A. J. Dessler, p. 1, Cambridge Univ. Press, New York.

Alexeev, I. I., and E. S. Belenkaya (2005), Modeling of the Jovian magnetosphere, *Ann. Geophys.*, *23*, 809.

Belcher, J. W. (1983), The low-energy plasma in the Jovian magnetosphere, in *Physics of the Jovian Magnetosphere*, edited by A. J. Dessler, p. 68, Cambridge Univ. Press, New York.

Belenkaya, E. S. (2004), The Jovian magnetospheric magnetic and electric fields: Effects of the interplanetary magnetic field, *Planetary Space Sci.*, *52*, 499.

Belenkaya, E. S., S. Y. Bobrovnikov, I. I. Alexeev, V. V. Kalegaev, and S. W. H. Cowley (2005), A model of Jupiter's magnetospheric magnetic field with variable magnetopause flaring, *Planet. Space Sci.*, *53*, 863.

Brown, M. E. (1994), Observations of mass loading in the Io plasma torus, *Geophys. Res. Lett.*, *21*, 847.

Bunce, E. J., and S. W. H. Cowley (2001), Divergence of the equatorial current in the dawn sector of Jupiter's magnetosphere: Analysis of Pioneer and Voyager magnetic field data, *Planet. Space Sci.*, *49*, 1089.

Bunce, E. J., S. W. H. Cowley, and T. K. Yeoman (2004), Jovian cusp processes: Implications for the polar aurora, *J. Geophys. Res.*, *109*, A09S13, doi:10.1029/2003JA010280.

Clarke, J. T., et al. (1998), Hubble Space Telescope imaging of Jupiter's UV aurora during the Galileo orbiter mission, *J. Geophys. Res.*, *103*, 20,217.

Clarke, J. T., D. Grodent, S. W. H. Cowley, E. J. Bunce, P. Zarka, J. E. P. Connerney, and T. Satoh (2004), Jupiter's auroras, in *Jupiter*, edited by F. Bagenal, T. E. Dowling, and W. B. McKinnon, p. 639, Cambridge Univ. Press, New York.

Connerney, J. E. P., M. H. Acuña, and N. F. Ness (1981), Modeling the Jovian current sheet and inner magnetosphere, *J. Geophys. Res.*, *86*, 8370.

Connerney, J. E. P., M. H. Acuña, N. F. Ness, and T. Satoh (1998), New models of Jupiter's magnetic field constrained by the Io flux tube footprint, *J. Geophys. Res.*, *103*, 11,929.

Cowley, S. W. H. (2000), Magnetosphere-ionosphere interactions: A tutorial review, in *Magnetospheric Current Systems*, *Geophys. Monogr. Ser.*, vol. 118, edited by S. Ohtani et al., pp. 91–106, AGU, Washington, USA.

Cowley, S. W. H., and E. J. Bunce (2001), Origin of the main auroral oval in Jupiter's coupled magnetosphere-ionosphere system, *Planet. Space Sci.*, *49*, 1067.

Cowley, S. W. H., and E. J. Bunce (2003a), Modulation of Jovian middle magnetosphere currents and auroral precipitation by solar wind-induced compressions and expansions of the magnetosphere: Initial conditions and steady state, *Planet. Space Sci.*, *51*, 31.

Cowley, S. W. H., and E. J. Bunce (2003b), Corotation-driven magnetosphere-ionosphere coupling currents in Saturn's magnetosphere and their relation to the auroras, *Ann. Geophys.*, *21*, 1691.

Cowley, S. W. H., J. D. Nichols, and E. J. Bunce (2002), Distributions of current and auroral precipitation in Jupiter's middle magnetosphere computed from steady-state Hill-Pontius angular velocity profiles: Solutions for current sheet and dipole magnetic field models, *Planet. Space Sci.*, *50*, 717.

Cowley, S. W. H., E. J. Bunce, and J. D. Nichols (2003a), Origins of Jupiter's main oval auroral emissions, *J. Geophys. Res.*, *108*(A4), 8002, doi:10.1029/2002JA009329.

Cowley, S. W. H., E. J. Bunce, T. S. Stallard, and S. Miller (2003b), Jupiter's polar ionospheric flows: Theoretical interpretation, *Geophys. Res. Lett.*, *30*(5), 1220, doi:10.1029/2002GL016030.

Cowley, S. W. H., E. J. Bunce, and R. Prangé (2004a), Saturn's polar ionospheric flows and their relation to the main auroral oval, *Ann. Geophys.*, *22*, 1379.

Cowley, S. W. H., E. J. Bunce, and J. M. O'Rourke (2004b), A simple quantitative model of plasma flows and currents in Saturn's polar ionosphere, *J. Geophys. Res.*, *109*, A05212, doi:10.1029/2003JA010375.

Elsner, R. F., et al. (2005), Simultaneous Chandra X ray, Hubble Space Telescope ultraviolet, and Ulysses radio observations of Jupiter's aurora, *J. Geophys. Res.*, *110*, A01207, doi:10.1029/2004JA010717.

Grodent, D., J. T. Clarke, J. Kim, J. H. Waite Jr., and S. W. H. Cowley (2003a), Jupiter's main oval observed with HST-STIS, *J. Geophys. Res.*, *108*(A11), 1389, doi:10.1029/2003JA009921.

Grodent, D., J. T. Clarke, J. H. Waite Jr., S. W. H. Cowley, J.-C. Gérard, and J. Kim (2003b), Jupiter's polar auroral emissions, *J. Geophys. Res.*, *108*(A10), 1366, doi:10.1029/2003JA010017.

Gustin, J., J.-C. Gérard, D. Grodent, S. W. H. Cowley, J. T. Clarke, and A. Grard (2004), Energy-flux relationship in the FUV Jovian aurora deduced from HST-STIS spectral observations, *J. Geophys. Res.*, *109*, A10205, doi:10.1029/2003JA010365.

Hill, T. W. (1979), Inertial limit on corotation, *J. Geophys. Res.*, *84*, 6554.

Hill, T. W. (2001), The Jovian auroral oval, *J. Geophys. Res.*, *106*, 8101.

Hill, T. W., and V. M. Vasyliunas (2002), Jovian auroral signature of Io's corotational wake, *J. Geophys. Res.*, *107*(A12), 1464, doi:10.1029/2002JA009514.

Hill, T. W., A. J. Dessler, and C. K. Goertz (1983a), Magnetospheric models, in *Physics of the Jovian Magnetosphere*, edited by A. J. Dessler, p. 353, Cambridge Univ. Press, New York.

Hill, T. W., A. J. Dessler, and M. E. Rassbach (1983b), Aurora on Uranus: A Faraday disc dynamo mechanism, *Planet. Space Sci.*, *31*, 1187.

Huang, T. S., and T. W. Hill (1989), Corotation lag of the Jovian atmosphere, ionosphere and magnetosphere, *J. Geophys. Res.*, *94*, 3761.

Isbell, J., A. J. Dessler, and J. H. Waite Jr. (1984), Magnetospheric energization by interaction between planetary spin and the solar wind, *J. Geophys. Res.*, *89*, 10,716.

Kane, M., B. H. Mauk, E. P. Keath, and S. M. Krimigis (1995), Hot ions in Jupiter's magnetodisc: A model for Voyager-2 low-energy charged particle measurements, *J. Geophys. Res.*, *100*, 19,473.

Khurana, K. K. (2001), Influence of solar wind on Jupiter's magnetosphere deduced from currents in the equatorial plane, *J. Geophys. Res.*, *106*, 25,999.

Knight, S. (1973), Parallel electric fields, *Planet Space Sci.*, *21*, 741.

Krupp, N., A. Lagg, S. Livi, B. Wilken, J. Woch, E. C. Roelof, and D. J. Williams (2001), Global flows of energetic ions in Jupiter's equatorial plane: First order approximation, *J. Geophys. Res.*, *106*, 26,017.

Laxton, N. F., A. Balogh, S. W. H. Cowley, M. W. Dunlop, R. J. Forsyth, R. J. Hynds, and K. Staines (1997), Origins of the first-order anisotropy of ~1 MeV protons in the Jovian magnetosphere during Ulysses flyby: Flux gradients and plasma flows, *Planet. Space Sci.*, *45*, 1143.

Lundin, R., and I. Sandahl (1978), Some characteristics of the parallel electric field acceleration of electrons over discrete auroral arcs as observed from two rocket flights, in *Symposium on European Rocket Research*, *ESA SP-135*, p. 125, Eur. Space Agency, Noordwijk, Netherlands.

Miller, S., et al. (2000), The role of H_3^+ in planetary atmospheres, *Phil. Trans. R. Soc. London, Ser. A*, *358*, 2485.

Millward, G., S. Miller, T. Stallard, A. D. Aylward, and N. Achilleos (2002), On the dynamics of the Jovian ionosphere and thermosphere III. The modelling of auroral conductivity, *Icarus*, *160*, 95.

Millward, G., S. Miller, T. Stallard, N. Achilleos, and A. D. Aylward (2005), On the dynamics of the Jovian ionosphere and thermosphere IV. Ion-neutral coupling, *Icarus*, *173*, 200.

Nichols, J. D., and S. W. H. Cowley (2003), Magnetosphere-ionosphere coupling currents in Jupiter's middle magnetosphere: Dependence on the effective ionospheric Pedersen conductivity and iogenic plasma mass outflow rate, *Ann. Geophys.*, *21*, 1419.

Nichols, J. D., and S. W. H. Cowley (2004), Magnetosphere-ionosphere coupling currents in Jupiter's middle magnetosphere: Effect of precipitation-induced enhancement of the ionospheric Pedersen conductivity, *Ann. Geophys.*, *22*, 1799.

Nichols, J. D., and S. W. H. Cowley (2005), Magnetosphere-ionosphere coupling currents in Jupiter's middle magnetosphere: Effect of magnetosphere-ionosphere decoupling by field-aligned auroral voltages, *Ann. Geophys.*, *23*, 799.

Pallier, L., and R. Prangé (2001), More about the structure of the high latitude Jovian aurorae, *Planet. Space Sci.*, *49*, 1159.

Pallier, L., and R. Prangé (2004), Detection of the southern counterpart of the northern polar cusp: Shared properties, *Geophys. Res. Lett.*, *31*, L06701, doi:10.1029/2003GL018041.

Phillips, J. L., S. J. Bame, B. L. Barraclough, D. J. McComas, R. J. Forsyth, P. Canu, and P. J. Kellog (1993a), Ulysses plasma electron observations of the Jovian magnetosphere, *Planet. Space Sci.*, *41*, 877.

Phillips, J. L., S. J. Bame, M. F. Thomsen, B. E. Goldstein, and E. J. Smith (1993b), Ulysses plasma electron observations in the Jovian magnetosheath, *J. Geophys. Res.*, *98*, 21,189.

Pontius, D. H., Jr. (1997), Radial mass transport and rotational dynamics, *J. Geophys. Res.*, *102*, 7137.

Pontius, D. H., Jr., and T. W. Hill (1982), Departure from corotation of the Io plasma torus: Local plasma production, *Geophys. Res. Lett.*, *9*, 1321.

Prangé, R., D. Rego, L. Pallier, J. E. P. Connerney, P. Zarka, and J. Queinnec (1998), Detailed study of FUV Jovian auroral features with the post-COSTAR HST faint object camera, *J. Geophys. Res.*, *103*, 20,195.

Rego, D., R. Prangé, and J. C. Gérard (1994), Lyman α and H_2 bands from the giant planets: 1. Excitation by proton precipitation in the Jovian aurorae, *J. Geophys. Res.*, *99*, 17,075.

Sands, M. R., and R. L. McNutt (1988), Plasma bulk flow in Jupiter's dayside middle magnetosphere, *J. Geophys. Res.*, *93*, 8502.

Satoh, T., J. E. P. Connerney, and R. L. Baron (1996), Emission source model of Jupiter's H_3^+ aurorae: A generalized inverse analysis of images, *Icarus*, *122*, 1.

Saur, J., B. H. Mauk, A. Kassner, and F. M. Neubauer (2004), A model for the azimuthal plasma velocity in Saturn's magnetosphere, *J. Geophys. Res.*, *109*, A05217, doi:10.1029/2003JA010207.

Scudder, J. D., E. C. Sittler Jr., and H. S. Bridge (1981), A survey of the plasma electron environment of Jupiter: A view from Voyager, *J. Geophys. Res.*, *86*, 8157.

Smith, C. G. A., S. Miller, and A. D. Aylward (2005), Magnetospheric energy inputs into the upper atmospheres of the giant planets, *Ann. Geophys.*, *23*, 1943.

Southwood, D. J., and M. G. Kivelson (2001), A new perspective concerning the influence of the solar wind on Jupiter, *J. Geophys. Res.*, *106*, 6123.

Stallard, T. S., S. Miller, S. W. H. Cowley, and E. J. Bunce (2003), Jupiter's polar ionospheric flows: measured intensity and velocity variations poleward of the main auroral oval, *Geophys. Res. Lett.*, *30*(5), 1221, doi:10.1029/2002GL016031.

Strobel, D. F., and S. K. Atreya (1983), Ionosphere, in *Physics of the Jovian Magnetosphere*, edited by A. J. Dessler, p. 51, Cambridge Univ. Press, New York.

Vasavada, A. R., et al. (1999), Jupiter's visible aurora and Io footprint, *J. Geophys. Res.*, *104*, 27,133.

Vasyliunas, V. M. (1983), Plasma distribution and flow, in *Physics of the Jovian Magnetosphere*, edited by A. J. Dessler, p. 395, Cambridge Univ. Press, New York.

Waite, J. H., Jr., T. E. Cravens, J. Kozyra, A. F. Nagy, S. K. Atreya, and R. H. Chen (1983), Electron precipitation and related aeronomy of the Jovian thermosphere and ionosphere, *J. Geophys. Res.*, *88*, 6143.

Waite, J. H., Jr., et al. (2001), An auroral flare at Jupiter, *Nature*, *410*, 787.

Yelle, R. V., and S. Miller (2004), Jupiter's thermosphere and ionosphere, in *Jupiter*, edited by F. Bagenal, T. E. Dowling, and W. B. McKinnon, p. 185, Cambridge Univ. Press, New York.

I. I. Alexeev, E. S. Belenkaya, and V. V. Kalegaev, Institute of Nuclear Physics, Moscow State University, Vorob'evy Gory, 119992 Moscow, Russia.

E. J. Bunce, C. E. Cottis, S. W. H. Cowley, J. D. Nichols, and F. J. Wilson, Department of Physics and Astronomy, University of Leicester, Leicester LE1 7RH, UK. (swhc1@ion.le.ac.uk)

R. Prangé, Observatoire de Paris, 5 place Jules Jansen, F-91370 Meudon, France.